MASTER'S THESIS

Mean field analysis of an effective lattice theory for isospin and baryonic chemical potential

AMINE BOUMEDIENNE CHABANE

JOHANN-WOLFGANG VON GOETHE UNIVERSITÄT
FRANKFURT AM MAIN
INSTITUT FÜR THEORETISCHE PHYSIK

Supervisor and first referee: Prof. Dr. Owe PHILIPSEN
Second referee: Prof. Dr. Francesca CUTERI

submitted on March 6, 2022

Contents

Abstract

The purpose of this Master's thesis is to establish two effective approaches for a $3+1$ Lattice QCD theory: In the first place, an effective theory by strong coupling and hopping parameter expansion up to $\mathcal{O}(\kappa^2)$ and subsequently a mean field ansatz will be applied for the order parameter $L_{\vec{x}}$ and the free energy $\mathcal{F}$ as well. In particular, this study is conducted for the full Wilson-Dirac action for $N_f = 1$ and $N_f = 2$ with the temporal lattice parameter $N_\tau = 10000$, which automatically corresponds to low temperature according to $T \propto [N_\tau]^{-1}$. Further, in the $N_f = 2$ case, the isospin μ_I and the baryonic chemical potential μ_B will be also incorporated into the derived effective theory, where afterwards μ_I and μ_B are modified as a combination. This leads to a novel phase diagram of (μ_I, μ_B), which reveals an interesting insight about the rich phase structure of QCD.

Chapter 1

Motivation

What is the universes really made of? What is truly fundamental in the reality that we perceive? In 400 BC, Greek philosopher Democritus came up with the idea of atoms (gr. $\alpha\tau o\mu\zeta$, "indivisible") as being fundamental. He believed that these were solid pieces of matter, which could not be divided any further. 2300 years later in in 1987 JJ Thompson discovered something smaller than an atom, called the electron and in 1912 Ernest Rutherford discovered that atoms had nuclei. Then we found that nuclei were composed of protons and neutrons, these were thought to be the fundamental components that all objects are made of, until the 1960s, when we found that neutrons and protons were composed of even smaller things called quarks. Today everything that we can see around us is thought to be made up of just these two particle species - electrons and quarks. However the only problem with this view - it's not true, and physicists know that. These particles are not really fundamental. Nature is made of fields and reality is fundamentally many of different fields. These objects which we called particles are merely waves in the field, they are convenient representations that are not really the best understanding of the universe today. These fields can be abstracted to fluid like substances that can be perturbed, vibrate or excited. But what are now exactly fields? Mathematically, a field is something that takes a value at every point in space. The idea that fields are a better representation that the original idea of particles lies on the key advantage that fields eliminates the idea of **action at the distance**, where for example in Newtonian gravity objects like the sun can somehow affects the earth, which is in fact far away. It was Albert Einstein and General Relativity, who eliminated the idea of action at a distance by replacing the conventional view of space, with something called **space-time**, which provides the space with a gravitational field. The problem that even Isaac Newton had was finally solved and the basic concept of fields became more and more popular in physics.

On Fig. 1.1 the Standard Model (SM) of particles is demonstrated, where basically two kinds of fundamental particles exist: The fermions (left blue column) and the bosons (right blue column). Fermions make up all the matter that we are aware of and the bosons are responsible for three fundamental interactions and the Higgs field. These are fundamental particles meaning in the current state of physics, the scientific community doesn't know anything smaller that they could be made of. Ordinary matter for example that we experience around us is just made of four of these particles: the up and down **quarks**, which make up the protons and neutrons in the nuclei of atoms, **electrons** which form a

cloud around the nucleus and the neutrino, which is created during the fusion process in stars like the sun. Naturally, there are also other particles, but they are rare and don't typically exist in ordinary matter, because these particles are created inside particles accelerators or from cosmic rays hitting the atoms in the atmosphere of earth. The reason why they don't exist in ordinary matter lies on the fact that these particles are very unstable and decay in fractions of a second (for example K^+ particle lifetime: $\tau_{K^+} = (1.2380 \pm 0.0020) \cdot 10^{-8}$ s). A good analogy for that are periodic table of the elements, where the heavy elements on the bottom of the table are also very rare because they tend to decay very quickly.

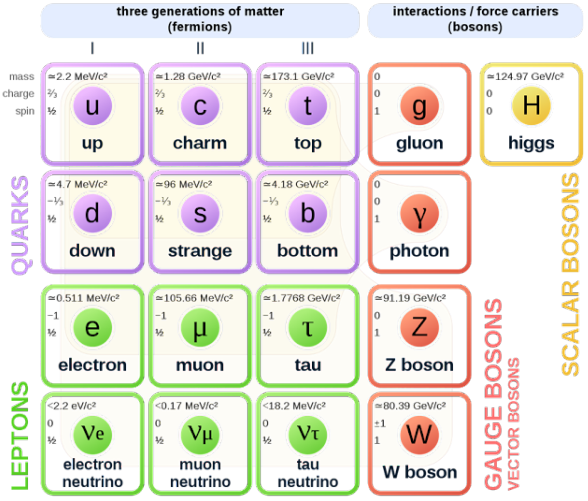

Figure 1.1: Standardmodell of particle physics. Figure taken from [1].

But lets stick on Fig. 1.1, where the fermions (left side) can be further divided into leptons and quarks. The biggest difference between quarks and leptons is that quarks interact with the strong nuclear interaction, which binds the nuclei of atoms together, whereas the leptons don't. The bosons on the right side are the interaction carriers: The photons γ carry the electromagnetic interaction responsible for all electricity, magnetism and chemistry. The W^+, W^- and Z^0 particles carry the weak interaction, which are responsible for weak decays (e.g. β^+/β^- decay) and the gluon g exhibits the strong nuclear interaction. Lastly we have the Higgs boson H, which is important for giving mass to all fundamental particles. The Standard Model is actually represented by a complex set of equations, but we can simplify all this in one equation known as the **Standard Model Lagrangian**

$$\begin{aligned}\mathcal{L} = &-\frac{1}{4}\mathcal{F}_{\mu\nu}\mathcal{F}^{\mu\nu} \\ &+ i\bar{\Psi}\gamma^{\mu}\mathcal{D}\Psi \\ &+ \mathcal{D}_{\mu}\Phi^{\dagger}\mathcal{D}^{\mu}\Phi - V(\Phi) \\ &+ \bar{\Psi}_L\hat{Y}\Phi\Psi_R + \text{h.c.}.\end{aligned}$$

Tab. 1.1 lists and explains selected properties about the known four fundamental interactions: Gravitation, electromagnetism, weak and strong interaction. In the current state of physics all this interaction, with the exception

of gravitation, can be described with a quantum field theory (QFT), which is a mathematical framework to integrate the basic idea of fields and connect classical physics, quantum mechanics and special relativity.

Lets focus on the strong interaction, because the corresponding theory, Quantum Chromodynamics (QCD) is the fundamental theory of this work. The corresponding particles to QCD are the quarks (see Tab 1.1) and physicist Gell Mann proposed that there were three types of quarks - up, down and strange quark. The up quark has a charge of $2/3$, whereas down and strange have a charge of $-1/3$ and they all experience the strong force. A proton for example is made of two up quarks and a down quark. The total charge is accordingly $Q = 2/3 + 2/3 - 1/3 \stackrel{!}{=} 1$ and other combinations of these quarks build other baryons like the neutron as well. The problem with this quark model is the following: According to quantum mechanics this should be impossible, because at least two of them would have the same quantum property. The rule behind this is the **Pauli Exclusion Principle**, where two or more identical fermions (like the up or down quarks) cannot occupy the same quantum state within a quantum system simultaneously. Finally the problem was solved in 1964, American physicist Greenberg proposed that quarks must have an **additional** property, which was not considered. This additional property is now called color and this has nothing to do with color that we can see with our eyes. It is a metaphor for a kind of charge, like the charge in the electromagnetic field, where just positive and negative charge exists. So if we consider now this new charge, the up quarks in the proton would not be identical, because all three quarks have different color charge and thus they would not violate the Pauli exclusion principle. Furthermore to get a "neutral" charge, we have to combine colors just like when we combine the visible colors red, green and blue to get a neutral white.

Table 1.1: The four fundamental interactions of nature.

	Gravitation	Weak	Electromagnetic	Strong
Mediating particles	Not observed	W^+ ,W^- and Z^0	γ-Photon	Gluons
Affected particles	All particles	Left-handed fermions	Electrically charged	Quarks, gluons
Acts on	Mass energy	Flavour	Electric charge	Color charge
Bound states formed	Planets, Stars, galaxies	-	Atoms, molecules	Hadrons
Affecting range [fm]	∞	$< 2 \cdot 10^{-3}$	∞	< 1
Coupling constant α_s	$5.76 \cdot 10^{-36}$	$\approx 1.01 \cdot 10^{-5}$	$\alpha_s \approx \frac{1}{137.036}$	$\alpha_s \sim 1$

After discussing the important property of color, the next astonishing property of QCD is quark confinement to explain that quarks must be confined somehow to within the nucleon. This implies that there must be something, which strongly holding these quarks together within the nucleon. This particle was called the gluon, because it acts like the glue that keeps the quarks together in the nucleon.

QCD deals with color charges and the mediating particle (see Tab 1.1) for it, which are the gluons. For comparison: In the electromagnetic interaction, the interaction particle will be the photon, which is massless as well. The difference between photons and gluons are that photons are electrically neutral so while they transmit the electromagnetic force, they do not experience it, nor do they interact with each other. The gluon, on the other hand, not only transmits the strong interaction, but also has a color charge itself, so it experiences the strong force as well.

This thesis is organized as the following: In Chpt. 2 we start with a brief overview over the QCD phase diagram, where we set our focus more on the lattice QCD (LQCD) results. After that, the complete Chpt. 3 is dedicated to the task to derive the effective theory, where especially the strong coupling limit and the hopping parameter expansion will be used. Furthermore, important expressions for the kinetic and static determinant are computed later in the ongoing Chapter. Once, the tools for the effective theory are explicitly ready, in Chpt. 4, those calculations will be extended with the mean field approach. The last Chpt. 5 finally draws some conclusion and significance of the results, and further gives an outlook on future research.

Chapter 2

QCD phase diagram

The aim of this chapter is to give a brief overview of the phase diagram of QCD, which is one of the most discussed and active areas in modern physics. This overview will rather focus on results of LQCD, which will also mean that due to the sign problem, results can only be relied on for zero baryonic chemical potential.

At first in Sec. 2.1, a brief overview about the conjectured QCD phase diagram in the (μ_B, T) plane will be disscued and after that the isospin chemical potential μ_I will be also introduced as a third axis on the QCD phase diagram. Then in Sec. 2.2 the QCD phase structure in the $(m_{u,d}, m_s)$ plane will be also considered in more detail, where results are only valid for $\mu_B = 0$. Naturally, there are more methods to analyze the QCD phase diagram, e.g. imaginary chemical potential [2], but in this respect we will not go any further. For a more detailed description, we refer the reader to the pedagogical introductions of Refs. [3, 4, 5] and references therein.

2.1 Conjectured QCD phase diagram

The study of the phase structure of Quantum Chromodynamics (QCD) at finite temperatures and baryon densities is one of the most important topics in modern physics. The importance for understanding the phase diagram comes from the fact that we still have experimental phenomena which we can't explain on a solid theoretical foundation. Not well understood phenomena are for example the expansion of the early universe, heavy-ion collisions in the Large-Hadron-Collider (LHC) or the properties and structure of neutron stars.

First of all the current state of the art of the QCD phase diagram is not well known, neither from a theoretical or experimental perspective. Despite this poor starting position Fig. (2.1) summarizes the current understanding of the QCD phase diagram, where the only important thermodynamic properties are the baryonic chemical potential μ_B and the temperature T. Let's start at the origin of the phase diagram at $T = 0$, $\mu_B = 0$ and then increasing the temperature (moving up vertically) slowly: In the beginning quarks will be still confined and they create a gas of hadrons. After a certain temperature the system reaches the crossover region to the quark gluon plasma, which is an interacting plasma of quarks and gluons. The temperature at the crossover is often refereed as the pseudo-critical line and is estimated to be in the range $T_{\text{pc}} \sim (150-200)$MeV [6, 7]. Furthermore, the early universe may also happened

in this scale, where after the Big-Bang there was a very tiny preference between matter and antimatter. The hadronic-quark-phase transition ($T = \mu = 0$) has been studied extensively on the lattice and the studies show for $N_c = 3$ and $N_f = 0$ a first order deconfinement transition [8].

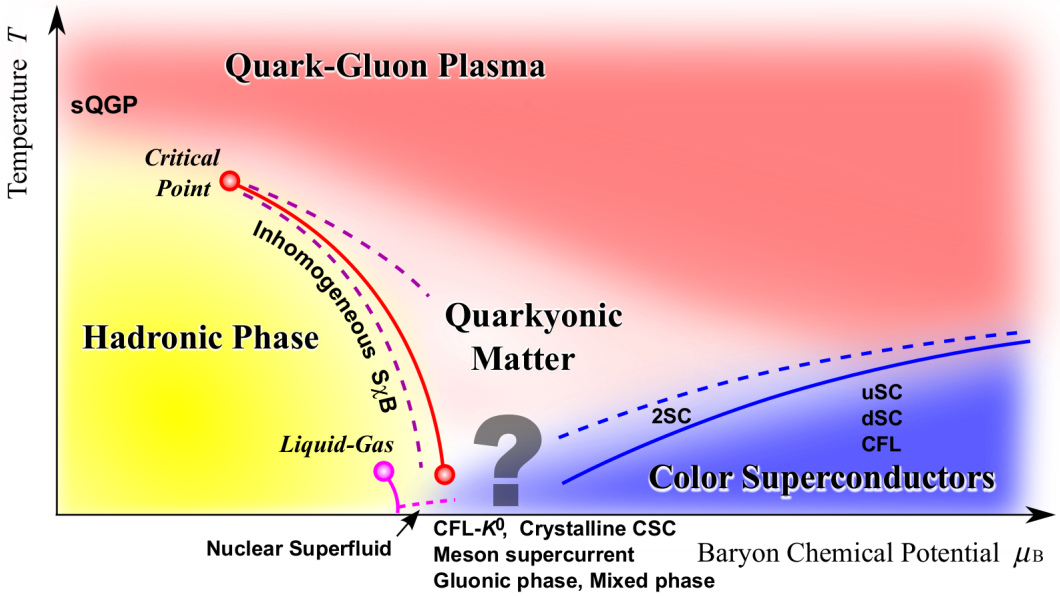

Figure 2.1: Schematic QCD phase based on the findings in chiral pertubation theory $S_\chi B$ [9]. The different transitions and phases are described in the tex. Figure taken from [5].

However, at finite densities μ the nature of the transition is not established yet. From first-principle LQCD calculation there is no reliable evidence about the critical endpoints of QCD. Despite this current state, they are chiral models, which are suggesting that critical point exists and the chiral transition becomes first order [10].

At $m \approx 939$MeV and growing T there is the conjecture that a first order transition occurs and ends up with a second order critical point (μ_c, T_c). This transition is often called as the liquid-gas transition. Low energy HIC experiments indicate this transition at $T_c \sim (15 - 20)$MeV [11]. Another conjectured phase structure of QCD is the colour superconductivity phase, which happens when μ is asymptotically large. The idea behind this phase is that like for Cooper-pairs in the BCS-theory the quark-quark will attract each other over the gluon. For comparison: In the BCS-theory electron pairs attract each other over phonons. Analogue to that the gluons with color-charge will gain mass, whereby the gluons without color-charge remain mass less.

There are several approaches to study the QCD phase diagram and one well established approach are Lattice-QCD (LQCD) simulations. In the limit of $T \geq 0$, $\mu_B = 0$ the behavior of QCD can be calculated with standard perturbation theory, because asymptotic freedom is a general feature of QCD, where quarks interact weakly at high energies and this is the reason why perturbation theory applies very good in this region [12].

However at finite chemical potential $\mu_R \neq 0$ the necessary Monte Carlo techniques can't be applied anymore, because these techniques have the goal

to evaluate the Feynmann path integral numerically and unfortunately the fermion determinant becomes a complex number at finite real μ_{R}. This is the point where the sign problem appears. There are different methods suggested to avoid the sign problem, but these methods are all restricted for a certain limit $(\mu_{\mathrm{R}}/T < 1)$ of the complex chemical potential (see Ref. [13] for more information).

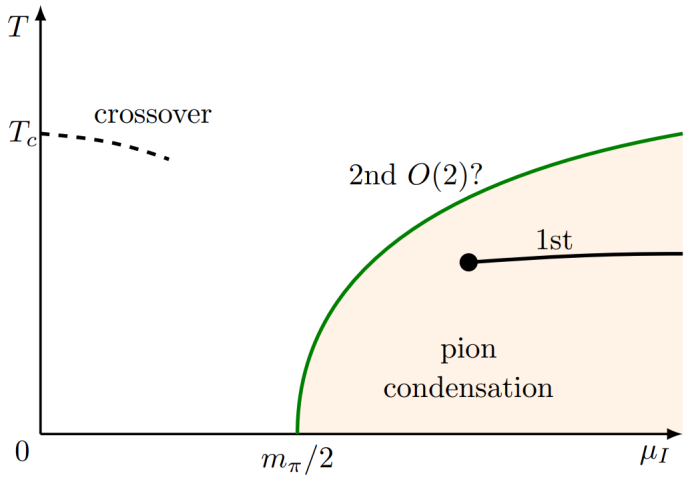

Figure 2.2: Schematic sketch of (μ_I, T)-plane of the QCD phase diagram. Figure taken from Ref. [14].

Another approach will be to introduce a imaginary chemical potential $\theta \equiv \mathrm{Im}\,\mu_{\mathrm{I}}/T$ to avoid the sign problem in a way that we still have the possibility to return back to real chemical potential via analytical continuation. Furthermore the symmetry of the light up (u) and down (d) quarks will be quit useful, to explore the phase structure of QCD in a different way. Fig. 2.2) shows the extension of the QCD-phase diagram with respect to the isospin chemical potential, where the isospin is defined as $\mu_{\mathrm{I}} = (\mu_{\mathrm{u}} - \mu_{\mathrm{d}})/2$ [14]. Of course at finite $\mu_{\mathrm{B}} \neq 0$ the sign problem remains, but for $\mu_{\mathrm{B}} = 0$ we have no sign problem anymore and standard Monte-Carlo simulations can be applied again. The resulting phase-diagram in the (T, μ_{I}) sector delivers us new insights about the structure of QCD, especially at $T = 0$ and small μ_{I} the "Silver-Blaze" phenomenon appears [15]. This property has the consequence that all thermodynimcal observables are independent of the chemical potential in the range of $\mu_B < \mu_c$, where $\mu_c = \mu_B - \epsilon$ (ϵ is the nuclear binding energy) is the threshold energy, which is even needed to produce a baryon at rest. In addition to that, if the system passes the chemical potential at $m_\pi/2$, charged pions arise and this will lead to pion condensation, where the conjectured phase transition is expected to be a second order phase transition [16].

2.2 The Columbia Plot

In the last section we summarized different aspects about the QCD phase diagram, as a function of temperature and matter density. Furthermore, the study was extended with the isospin chemical potential μ_I as well and new insights about the QCD phase structure was revealed. Now, there is also the reason to

still further extend the study with the up and down $m_{u,d}$ (considered as degenerate for simplicity) and strange m_s quark masses for $\mu_B = 0$. This consideration is completely projected along the T-axis of the QCD phase diagram, which was mentioned in Fig. 2.1.

The fact that recent lattice studies focused at $\mu_B = 0$ lies due to challenging field of QCD to solve or bypass the sign problem, because as we already know the infamous sign problem makes numerical simulations impossible. According to the current state of this studies, all of them can be more or less summarized in Fig. 2.3, which is often refereed as the Columbia plot [17].

First of all, the Columbia plot, as already mentioned, describes in general the masses of the up and down quark on the x-axis and on the y-axis the mass of the strange quark. Furthermore, one special feature of the Columbia plot is that the plot exhibits different flavor cases of the quarks: On the right axis of Fig. 2.3, the $N_f = 1$ is considered and the masses for the degenerate up and down quarks are $m_{u,d} = \infty$, where on the upper axis for $N_f = 2$ the mass for the strange quark goes to infinity. The last flavor case, namely $N_f = 3$, is illustrated, if you directly move on the diagonal of the Columbia plot. The Physical Point, however, is located on the special case for $N_f = 2 + 1$, where on this case the $m_{u,d}$ and m_s up posses different masses.

Nevertheless, strictly speaking the Columbia plot is not a phase diagram after all, because there are regions, which are not referring themselves as phases of matter. The necessity that the Columbia plot becomes a phase diagram in a way lies on the fact that the temperature axis is projected on the Columbia plot, which automatically means that each point on the plot corresponds to a critical value of the temperature. In general each color and position of the lines on the Columbia plot are separating regions, which are all indicating possible order of the phase transitions.

First we start with the infinity mass limit $m_{u,d}, m_s \to \infty$ (upper right corner of Fig. 2.3) and this is the point where the pure Yang-Mills theory is recovered: However, in this case the global $Z(3)$ symmetry breaks and the corresponding order parameter is the absolute value of the Polyakov Loop $\langle |L| \rangle$. In the opposite limit $m_{u,d}, m_s \to 0$ (lower left corner of Fig. 2.3) along the diagonal, the chiral limit takes place, because all masses are shrinking to zero and it is clear that at some point the temperature will restore the global chiral symmetry, at least for the subgroup $SU_L(N_f) \times SU_R(N_f)$. It is known that an order parameter for the chiral limit is the chiral condensate, which is defined as $\langle \bar{\psi}, \psi \rangle$. To conclude with, in the chiral limit, things are more difficult as in the infinity mass limit, because no simulation is possible. However, there are some methods to circumvent the problem, which are all based on analysis using the epsilon expansion about $\epsilon = 1$ applied to a linear sigma model in three dimensions [18].

Let's still stick to the Columbia plot, because so far only two points in an entire plane were discussed. Next, we take a close look to the chiral Z_2 boundaries, which are the blue lines in Fig. 2.3 that are separating first order regions from a much greater crossover regions. Here, we have reasons to believe that the transition is first order for pure Yang Mills theory (upper right corner) as according to the famous "Svetitsky-Yaffe conjecture" [19], where the conjecture predicts that a $(d + 1)$ dimensional pure gauge theory undergoes a deconfinement transition, which is comparable to a d- dimensional statistical model with an order parameter, which is also part of the center of the gauge group. Similar

study was done in the chiral limit of three flavors $N_f = 3$, based on an analysis by Ref. [20]. The other thing we know for sure is that a first order phase transition can not be isolated in a strict manner. This means that "The Jump" of the order parameter must be absorbed and becomes smaller in the long way and finally goes to zero [21]. As a logical consequence, this will correspond to tuning of the value of the corresponding symmetry breaking field, which is respectively the mass.

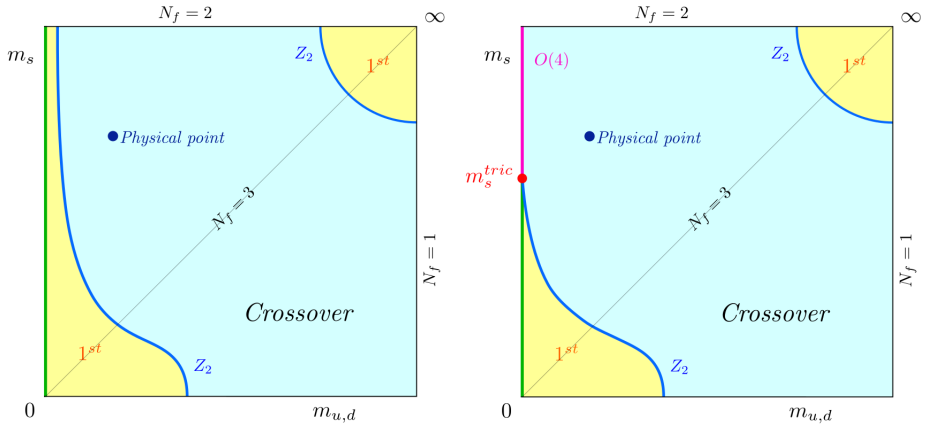

Figure 2.3: The phase structure of Lattice QCD at zero chemical potential. Two different scenarios for the Columbia plot, both plots are shown in the $m_s - m_{u,d}$ plane. Figure taken from Ref. [22].

Many aspects of Fig. 2.3 are studied with lattice simulations: One for example is the width of the chiral phase order region, where the region grows as a function with the number of fermionic species in the simulation [23]. It is not yet clear if there is a finite size of the chiral region at $N_f = 2$ and an important role could be played by the effective $U_A(1)$ restoration at T_c, because that tells you how much symmetry the system has and whether we should expect to have a first order or rather a second order transition [24].

Finally the Columbia plot is not based on continuum extrapolated results, the only point which safely can be located is the physical point, where we know that there is a crossover and not a true phase transition [25]. The physical point corresponds to the quark masses found in nature and is the only point in the Columbia plot, which is directly related to the QCD phase diagram (Fig. 2.1). This point corresponds to $\mu_B = 0$ and $T_c \approx 150 MeV$.

Another important remark is that up and down quark masses are very small and therefore the question remains, where the physical point is affected by remnants of the chiral universality class, especially if this region shrinks to zero. This will lead then to a second order phase transition in which the universality is in place. This discussion becomes relevant when we want to switch on a non zero chemical potential and a symmetry between the density of matter and antimatter, where we you can build a three dimensional version of the Columbia plot. Depending on the behavior of the blue line in the chiral limit in Fig. 2.3, which bends surfaces in the 3d Columbia plot, we can argue about the existence or non existence of the second order critical endpoint, which is one of the most important points for the characteristics of the QCD phase diagram in the (T, μ_B) plane [26]. So we can clearly see that especially the 3d Columbia plot can be very interesting to understand the QCD phase diagram, because it is

also deeply connected to the QCD phase diagram via the chemical potential.

Overall the order of the chiral transition in the lower left corner of Fig. 2.3 for $N_f = 1$ and $N_f = 3$ are still under debate and many possible scenarios are in discussion. Further, there are still two possible scenarios for the nature of $N_f = 2$ chiral transition.

Chapter 3

Derivation of the Effective Theory

LQCD is a non-perturbative approach to QCD based on a discretization of space-time. It is a lattice gauge theory formulated on a grid or network of points in space and time. On the theory side, one well established approach is perturbation theory which, however, only works at high temperatures, where quarks interact weakly due to the asymptotic freedom property of QCD. In the strongly interacting regime, the phase diagram can be investigated by means of lattice QCD simulations. The corresponding Monte Carlo techniques can only be applied for zero (or purely imaginary) chemical potentials. For $\mathrm{Re}\,\mu_B \neq 0$ the fermion determinant becomes complex and the so called sign problem appears. There are different methods suggested to circumvent the sign problem, but most of these methods are restricted to work at $\mu_B/T \geq 1$ (see e.g. Refs. [13, 27, 28] for reviews).

The aim of this chapter is now to derive an effective theory, which will determine important properties of lattice QCD in a relevant parameter region ((μ_B, T) region for example) and to mitigate the infamous sign problem in the best possible way, since numerical simulations do not work if the sign problem still exists. Another important advantage that the effective theory reveals, is the possibility to approach LQCD from an analytical standpoint, which was not directly possible in advance. To see the advantage, we will first start deriving the theory over the path integral formalism of Lattice QCD [29]:

$$\boxed{\mathcal{Z}_{\mathrm{LQCD}} = \prod_{f=1}^{N_f} \int [\mathrm{d}U_\mu]\, \det Q_f[U_\mu]\, e^{-S_g[U_\mu]}}. \tag{3.1}$$

The above equation is the starting point of our theory, which is why it will be important to understand all the components of this equation exactly.

- $S_g[U_\mu]$ is the lattice gauge action and is defined as

$$S_g[U_\mu] = \frac{\beta}{2N_c} \sum_P \mathrm{Tr}\Big(U_P + U_P^\dagger\Big).$$

  The parameter β is the inverse lattice gauge coupling and takes form $\beta = \frac{2N_c}{g^2}$, where N_c is the number of colors and g is the coupling constant. The

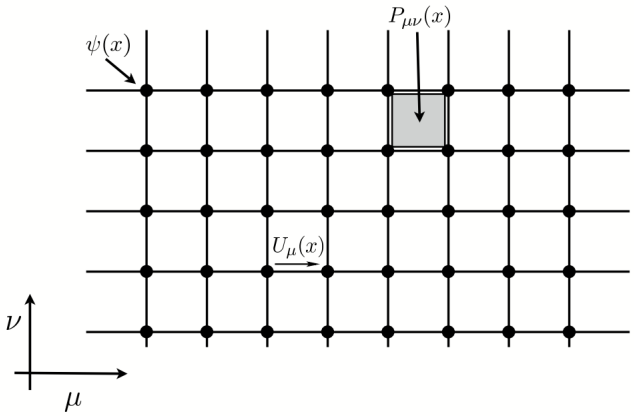

Figure 3.1: Two dimensional lattice with the plaquette $P_{\mu\nu}(x)$. Figure taken from [30].

expression U_P is the simplest closed loop on the lattice, called plaquette and has the form (cf. Fig. 3.1 for a visual representation).

$$U_P \equiv P_{\mu\nu} = U_\mu(x)\, U_\nu(x+\mu)\, U_\mu^\dagger(x+\nu) U_\mu^\dagger(x).$$

- $\det Q^f[U_\mu]$ is the quark (or fermion) determinant and follows from the fact that fermion fields are formulated in terms of Gassmann numbers and integrating them out leads to the relation [29]

$$\int \mathrm{d}\eta_1^\dagger \mathrm{d}\eta_1 \ldots \mathrm{d}\eta_N^\dagger \mathrm{d}\eta_N \exp\left[-\sum_{i,j} \eta_j^\dagger A_{ij} \eta_i\right] \stackrel{!}{=} \det A,$$

  where the origin of the determinant in Eq. (3.1) becomes clear.

In addition, another very important quantity in Eq. (3.1) is the Wilson-Dirac operator $Q[U]$, whose origin lies in the Wilson-Dirac action. To see this in more detail, we start with the Wilson-Dirac action

$$\begin{aligned} S_W\left[\psi, \overline{\psi}, U\right] = \sum_{f=1}^{N_f} a^4 \sum_{x,y\in\lambda} \overline{\psi}^f(x) \Bigg[\left(m^f + \frac{4}{a}\right)\delta_{x,y} \\ - \frac{1}{2a}\sum_{\mu=0}^{3} \left[(\mathbb{1}-\gamma_\mu) U_\mu(x)\delta_{x+\hat{\mu},y} + (\mathbb{1}+\gamma_\mu) U_\mu(x)\delta_{x,y+\hat{\mu}}\right] \Bigg] \psi^f(y). \end{aligned} \tag{3.2}$$

For further calculation the hopping parameter $\kappa^f = \left[2am^f + 8\right]^{-1}$ is introduced, so the Wilson-Dirac action can be rewritten in

$$
\begin{aligned}
S_W\left[\psi,\overline{\psi},U\right] &= \sum_{f,x,y} a^4 \frac{1}{2a\kappa^f}\psi^f(x)\left[\delta_{x,y} - \kappa^f \sum_{\mu=0}^{3}\left[(\mathbb{1}-\gamma_\mu)U_\mu(x)\delta_{x+\hat{\mu},y} + (\mathbb{1}+\gamma_\mu)U_\mu(x)\delta_{x,y+\hat{\mu}}\right]\right]\psi^f_{(x)} \\
&= \sum_{f=1}^{N_f}\sum_{x,y\in\lambda}\frac{a^2}{\sqrt{2a\kappa^f}}\,\frac{a^2}{\sqrt{2a\kappa^f}}\psi^f(x)\underbrace{\left[\mathbb{1}-\kappa^f H(x,y)\right]}_{\equiv Q^f(x,y)}\psi^f(y) \\
&= \sum_{f=1}^{N_f}\sum_{x,y\in\lambda}\psi^f(x)Q^f(x,y)\psi(y),
\end{aligned}
$$

where

$$
Q^f(x,y) \equiv \mathbb{1} - \kappa^f H(x,y) \tag{3.3}
$$

is the mentioned Wilson-Dirac operator. Here, also the fact was exploited that the Wilson-Dirac action contains the freedom of field normalization, therefore $\frac{a^2}{\sqrt{2a\kappa^f}}\psi^f(x) \rightarrow \psi^f(x)$ can be used. Moreover, the Wilson-Dirac operator contains also the so called hopping matrix $H(x,y)$, which takes the form

$$
H(x,y) = \sum_{\mu=0}^{3}\left[(\mathbb{1}-\gamma_\mu)U_\mu(x)\delta_{x+\hat{\mu},y} + (\mathbb{1}+\gamma_\mu)U_{-\mu}(x)\delta_{x,y-\hat{\mu}}\right]. \tag{3.4}
$$

In the next step we will rewrite the partition function in Eq. (3.1) in order to split the integral in temporal and spatial contributions.

$$
\mathcal{Z} = \prod_{f=1}^{N_f}\int [\mathrm{d}U_\mu]\det Q^f\; e^{-S_g} \tag{3.5}
$$

$$
= \prod_{f=1}^{N_f}\int [\mathrm{d}U_0]\int [\mathrm{d}U_i]\det Q^f e^{-S_g} \tag{3.6}
$$

$$
\Rightarrow \mathcal{Z}_{\text{eff}} = \int [\mathrm{d}U_0]\, e^{-S_{\text{eff}}}, \tag{3.7}
$$

with the effective action

$$
-S_{\text{eff}} = \ln\int [\mathrm{d}U_i]\left[\det Q^f\; e^{-S_g}\right]. \tag{3.8}
$$

Now, the advantage is that we can define $\int[\mathrm{d}U_0] \rightarrow \int[\mathrm{d}L]$ as the integration measure, where L stands for the Polyakov-Loop and takes the form $L(\vec{\mathbf{x}}) = \mathrm{Tr}\, W(\vec{\mathbf{x}}) = \mathrm{Tr}\prod_{\tau=0}^{N_\tau-1} U_0(\vec{\mathbf{x}},\tau)$. The above derived equation is now our starting point for further calculations, where the fermion determinant and pure gauge action will be expanded in a certain way and finally expressed with the Polyakov-Loop.

3.1 The Character Expansion

In the strong coupling limit lattice gauge theory corresponds to a statistical system at high temperature, because as we already know from the last section, the lattice gauge coupling constant takes the form $\beta = \frac{2N_c}{g^2}$, which directly shows the dependency between $g^2 \propto \frac{1}{\beta}$. From this relation, one can conclude, if $g \to \infty$ automatically $\beta \to 0$ and finally the weight factor $e^{-S_g} \to 1$, which is just the assumption of the so called strong coupling expansion. At this point, we will not go into more detail (see Ref. [31, 32] for more information) and will directly use the character expansion for the weight factor from Eq. (3.8). We start with

$$\begin{aligned} e^{-S_g} &= \exp\left[\beta \frac{1}{2N_c} \sum_P \left(\operatorname{Tr} U_P + U_P^\dagger\right)\right] \\ &= \prod_P \exp\left[\beta \chi(U_P)\right] \\ &= \prod_P \left[1 + \beta\chi(U_P) + \frac{\beta^2}{2}\chi^2(U_P) + \dots\right] \end{aligned}$$

where in the last step the series expansion was used. Next, the character expansion comes into action, which is why we can reformulate the weight factor in the following way [33]:

$$\begin{aligned} \Longrightarrow \quad e^{-S_g} &\stackrel{!}{=} \sum_r d_r c_r(\beta) \chi_r(U_P) \\ &= c_0(\beta)\left[1 + \sum_{r\neq 0} d_r \underbrace{\frac{c_r(\beta)}{c_0(\beta)}}_{=a_r(\beta)} \chi_r(U_P)\right] \\ &= c_0(\beta)\left[1 + \sum_{r\neq 0} d_r a_r(\beta) \chi_r(U_P)\right] \end{aligned}$$

where d_r is the dimension of the representation, $\chi_r(U)$ character of a representation and $a_r(\beta)$ the corresponding expansion parameter. Note that the sum $\sum_{r\neq 0}$ extends over all nontrivial irreducible representation at this point. With this result, the effective action in Eq. (3.8) can be reformulated in the following way

$$-S_{\text{eff}}^g = \ln \int [\mathrm{d}U_i] \prod_P \left[1 + \sum_r d_r a_r(\beta) \chi_r(U_P)\right] \tag{3.9}$$

Two different things are important here: First the coefficient $c_0(\beta)$ has been factored out and neglected, because the coefficient is constant and second the quark contribution has been ignored for this purpose, because it is possible to handle the pure gauge action alone and then in the end to insert the emerging result in the effective action. Now we only have to perform the spatial integration to finally get the result. Before doing so, the group integral

$$\int \mathrm{d}U \chi_r(XU)\ \chi_s\big(U^{-1}Y\big) = \frac{\delta_{rs}}{d_r}\chi_r(XY) \tag{3.10}$$

must be utilized first [34]. Trough this integration, the final result for the effective action is

$$-S^g_{\text{eff}} = \ln \prod_{\langle \vec{\mathbf{x}},\vec{\mathbf{y}}\rangle} \left[1 + \sum_r d_r [a_r(\beta)]^{N_\tau} \chi_r(W_{\vec{\mathbf{x}}})\chi_r\left(W^\dagger_{\vec{\mathbf{y}}}\right)\right]. \tag{3.11}$$

which is the nearest neighbour interaction between Polyakov-Loops in all representations (note that the product $\prod_P$ can be replaced by a product over nearest neighbour sites $\prod_{\langle \vec{\mathbf{x}},\vec{\mathbf{y}}\rangle}$). Furthermore we also remark that the effective action was reduced with functions of the Polyakov-Loop, which takes the form $L(\vec{\mathbf{x}}) = TrW_{\vec{\mathbf{x}}} \equiv \prod_{\tau=1}^{N_\tau} U_0(\vec{\mathbf{x}},\tau)$.

The leading order of the pure gauge action is given by the fundamental and anti-fundamental expression and the expansion parameter $a_r(\beta) \equiv u$ and the effective coupling $\lambda_1 \equiv u^{N_\tau} + \mathcal{O}\big(\beta^2\big)$. So now, the nearest neighbour pure gauge action only depends on functions of the Polyakov-Loop. This leads to

$$-S^{\text{g}}_{\text{eff}} = \sum_{\langle \vec{\mathbf{x}},\vec{\mathbf{y}}\rangle} \ln\left[1 + \lambda_1\left(L^\star_{\vec{\mathbf{x}}}L_{\vec{\mathbf{y}}} + L_{\vec{\mathbf{x}}}L^\star_{\vec{\mathbf{y}}}\right)\right]. \tag{3.12}$$

Higher orders of the strong coupling expansion for λ_1 can be looked up in the Appendix A.1 (cf. Eq. (A.3)).

3.2 The Hopping Parameter Expansion

After the effective theory in their pure gauge sector has been expanded in the strong limit, the next step is to investigate the emerging quark determinant, which is clearly the fermion contribution of the efffective theory. It is important to mention, that we will expand the quark determinant around heavy quarks (i.e. $\kappa^f \to 0$) and the strong coupling expansion from last section is still valid.

To start with, the Wilson-Dirac operator from Eq. (3.3) will be reinserted in the fermion determinant

$$\begin{aligned}
\det Q^f &= \det\left[\mathbb{1} - \kappa^f H(x,y)\right] \\
&= \exp \mathrm{Tr} \ln\left[\mathbb{1} - \kappa^f H(x,y)\right] \\
&= \exp\left[-\sum_{n=0}^{\infty} \frac{\left(\kappa^f\right)^n}{n} \mathrm{Tr}\, H^n(x,y)\right],
\end{aligned}$$

where we have used the expansion of the logarithm and the trace-log identity

$$\det \mathcal{A} = \exp \mathrm{Tr} \ln \mathcal{A}. \tag{3.13}$$

For the expansion above, it is possible to say that due to the definition of the hopping matrix $H(x,y)$, every contribution comes along with a Kronecker delta $\delta_{y,x\pm\hat{\mu}}$ and this can be interpreted as a single hop on the lattice, where also each hop has a regular spin factor of $(1\pm\gamma_\mu)$. However after tendering the sum in the expansion, terms with the shape of $(1-\gamma_\mu)(1+\gamma_\mu)$ will vanish, because no backtracing on the lattice is allowed. Therefore the expansion provides only closed fermion loops with a length of n.

Now, after the framework is clear, the Wilson-Dirac operator from Eq. (3.3) will be slightly modified in a way to also include the chemical potential μ into the theory. Before doing so, the Wilson-Dirac operator will be splitted into temporal and spatial parts:

$$\begin{aligned} Q^f(x,y) &= \mathbb{1} - \kappa \sum_{\mu=0}^{3} \left[(\mathbb{1}-\gamma_\mu)U_\mu(x)\delta_{x+\hat{\mu},y} + (\mathbb{1}+\gamma_\mu)U_{-\mu}(x)\delta_{x,y-\hat{\mu}}\right] \\ &= \mathbb{1} - \kappa\Bigg[(\mathbb{1}-\gamma_0)\,U_0\,\delta_{x+\hat{0},y} + (\mathbb{1}+\gamma_0)\,U_0^\dagger\,\delta_{x,y+\hat{0}} \\ &+ \sum_{i=1}^{3}\left[(\mathbb{1}-\gamma_i)\,U_i\,\delta_{x+\hat{i},y} + (\mathbb{1}+\gamma_i)\,U_i^\dagger\,\delta_{x,y+\hat{i}}\right]\Bigg] \end{aligned} \tag{3.14}$$

Here the fact was used that $U_{-\mu} = U^\dagger$. Next, to finally implement the chemical potential μ^f into the equation, the transformation $U_\mu \to \exp\left[a\mu^f\delta_{\mu,\hat{0}}\right]U_\mu$ and $U_\mu^\dagger \to \exp\left[a\mu^f\delta_{-\mu,\hat{0}}\right]U_\mu^\dagger$ must be performed out (see e.g. Ref. [29] for more information). Finally the Wilson-Dirac operator becomes:

$$\begin{aligned} Q^f(x,y) = \mathbb{1} - \kappa\Bigg[&e^{a\mu^f}(\mathbb{1}-\gamma_0)\,U_0\,\delta_{x+\hat{0},y} + e^{-a\mu^f}(\mathbb{1}+\gamma_0)\,U_0^\dagger\,\delta_{x,y+\hat{0}} \\ &+ \sum_{i=1}^{3}\left[(\mathbb{1}-\gamma_i)\,U_i\,\delta_{x+\hat{i},y} + (\mathbb{1}+\gamma_i)\,U_i^\dagger\,\delta_{x,y+\hat{i}}\right]\Bigg]. \end{aligned} \tag{3.15}$$

After splitting the Wilson-Dirac Operator into the space-time hops and extending it with the chemical potential, the hopping matrix from Eq. (3.4) will be also splitted in the spatial and temporal hops, because those quantities are connected via (3.3). So, it follows

$$H(x,y) = \underbrace{T_{xy}^+ + T_{xy}^-}_{\equiv T} + \sum_{i=1}^{3}\left[\underbrace{S_{xy,i}^+ + S_{xy,i}^-}_{\equiv S}\right], \tag{3.16}$$

where the spatial $S \equiv S_{x,y,i}^+ + S_{x,y,i}^-$ and temporal $T \equiv T_{x,y}^+ + T_{x,y}^-$ hops were introduced. Those hops are defined as

$$\begin{aligned} T_{x,y}^+ &= e^{a\mu}(\mathbb{1}+\gamma_0)\,U_0(x)\,\delta_{y,x+\hat{0}} \\ T_{x,y}^- &= e^{-a\mu}(\mathbb{1}-\gamma_0)\,U_0^\dagger(y)\,\delta_{y,x-\hat{0}} \\ S_{x,y}^+ &= (\mathbb{1}-\gamma_i)\,U_i(x)\,\delta_{y,x+\hat{i}} \\ S_{x,y}^- &= (\mathbb{1}+\gamma_i)\,U_i^\dagger(x)\,\delta_{y,x-\hat{i}}. \end{aligned} \tag{3.17}$$

After all these considerations, we jump back to the fermion determinant, which was first defined in Eq. (3.8) and rewrite the complete expression in the following way

$$\begin{aligned}\det Q^f &= \det\left[\mathbb{1} - \kappa\, H(x,y)\right] \\ &= \det\left[\mathbb{1} - \kappa\, T - \kappa\, S\right] \\ &= \det\left[(\mathbb{1} - \kappa\, T)\left(\mathbb{1} - \frac{\kappa\, S}{\mathbb{1} - \kappa\, T}\right)\right]\end{aligned}$$

$$\implies \quad \det Q_f = \underbrace{\det\left(\mathbb{1} - \kappa\, T\right)}_{\det Q_{\text{stat}}} \underbrace{\det\left(\mathbb{1} - \frac{\kappa\, S}{\mathbb{1} - \kappa\, T}\right)}_{\det Q_{\text{kin}}}. \tag{3.18}$$

Note, that in the limit of static (or infinitely heavy quarks) only temporal hops will contribute, whereby on the kinetic determinant also a spatial contribution appears, which can be interpreted as a correction term. Since, those quantities are important for further calculations, the next two sections will address the question of how the Polyakov-Loop can be expressed into the static and kinetic determinant as well.

3.3 Static Quark Determinant

As we know by now, the determinant is composed of a kinetic and a static one. In this chapter we look at the static determinant again more exactly, which is defined according to equation Eq. (3.18). Or in other words, the goal is to express the determinant with Polyakov loops because they can be better computed later.

$$\begin{aligned}\det Q_{\text{stat}} &\equiv \det\left(\mathbb{1} - \kappa T\right) \\ &= \exp \operatorname{Tr} \log\left(\mathbb{1} - \kappa T\right) \\ &= \exp \operatorname{Tr}\left\{\sum_{n=1}^{\infty} \frac{\kappa^n}{n} T^n\right\} \\ &= \exp \operatorname{Tr}\left\{\sum_{n=1}^{\infty} \frac{\kappa^n}{n} \left(T^+ + T^-\right)^n\right\}\end{aligned}$$

Here we have used the relation in Eq. (3.13) to rewrite the determinant and after that the series expansion $\log(1-\mathcal{A}) = \sum_{n=1}^{\infty} \frac{\mathcal{A}^n}{n}$ of the logarithm. Due to the fact that backtracking is not allowed and the mixed terms T^+T^- give no contribution, the last expression in Eq. (3.19) $(T^+ + T^-)^n \approx (T^+)^n + (T^-)^n$ can be simplified in the following way

$$\begin{aligned}\implies \det Q_{\text{stat}} &= \exp\left[\operatorname{Tr}\left\{\sum_{n=1}^{\infty} \frac{\kappa^n}{n}\left(T^+\right)^n\right\}\right] \exp\left[\operatorname{Tr}\left\{\sum_{n=1}^{\infty} \frac{\kappa^n}{n}\left(T^-\right)^n\right\}\right] \\ &= \det\left[\mathbb{1} - \kappa T^+\right] \det\left[\mathbb{1} - \kappa T^-\right].\end{aligned}$$

The identity in Eq. (3.13) was used again. Since our goal is to include the Polyakov loops in the determinant, we need to insert the temporal hops from Eq. (3.17) next, as these are necessary to then extract the Polyakov loops from them. Thus we can write

$$\det Q_{\text{stat}} = \prod_{\vec{\mathbf{x}}} \det\left[\mathbb{1} + \frac{1}{2}(2\kappa)^{N_\tau} e^{N_\tau a\mu}(\mathbb{1}+\gamma_0) W_{\vec{\mathbf{x}}}\right] \det\left[\mathbb{1} + \frac{1}{2}(2\kappa)^{N_\tau} e^{-N_\tau a\mu}(\mathbb{1}+\gamma_0) W^\dagger_{\vec{\mathbf{x}}}\right] \tag{3.19}$$

$$= \prod_{\vec{\mathbf{x}}} \det\left[\mathbb{1} + \underbrace{(2\kappa)^{N_\tau} e^{N_\tau a\mu}}_{\equiv h(\mu, N_\tau)} W_{\vec{\mathbf{x}}}\right]^2 \det\left[\mathbb{1} + \underbrace{(2\kappa)^{N_\tau} e^{-N_\tau a\mu}}_{\equiv \bar{h}_1(\mu, N_\tau)} W^\dagger_{\vec{\mathbf{x}}}\right]^2 \tag{3.20}$$

$$\implies \det Q_{\text{stat}} = \prod_{\vec{\mathbf{x}}} \left(\mathbb{1} + h_1 L_{\vec{\mathbf{x}}} + h_1^2 L^\dagger_{\vec{\mathbf{x}}} + h_1^3\right)^2 \left(\mathbb{1} + \bar{h}_1 L^\dagger_{\vec{\mathbf{x}}} + \bar{h}_1^2 L_{\vec{\mathbf{x}}} + \bar{h}_1^3\right)^2. \tag{3.21}$$

To get Eq. (3.21) we used the Relation $\det(\mathbb{1} + \alpha A) = 1 + \alpha \operatorname{Tr}(A) + \alpha^2 \operatorname{Tr}\left(A^\dagger\right) + \alpha^3$ for the special case when $A \in SU(3)$ [35]. Afterwards the definition $L_{\vec{\mathbf{x}}} \equiv L(\vec{\mathbf{x}}) = \operatorname{Tr} W(\vec{\mathbf{x}})$ and $L^\dagger_{\vec{\mathbf{x}}} \equiv L^\dagger(\vec{\mathbf{x}}) = \operatorname{Tr} W^\dagger(\vec{\mathbf{x}})$ have been inserted. Important quantities from Eq. (3.21) are

$$h_1(\mu, N_\tau) \equiv (2\kappa)^{N_\tau} e^{N_\tau a\mu} \qquad (3.22)$$
$$\overline{h}_1(\mu, N_\tau) \equiv (2\kappa)^{N_\tau} e^{N_\tau a\mu},$$

which are the effective quark coupling of the effective theory. In the entire effective theory, the quark coupling, which is defined above will describe the quarks and anti-quarks, where for instance $\overline{h}_1$ represent the anti-quarks. Furthermore, we remark that the integration for the static determinant will be trivial, because spatial links have been neglected. Therefore we can write the partition function as

$$\begin{aligned} \mathcal{Z} &= \int [\mathrm{d}U_0] \exp\left[\int \mathrm{d}U_i \; S_{\text{stat}}\right] \qquad (3.23) \\ &= \int [\mathrm{d}U_0] \left\{ \prod_{\vec{\mathbf{x}}} \left(\mathbb{1} + h_1 L_{\vec{\mathbf{x}}} + h_1^2 L_{\vec{\mathbf{x}}}^\dagger + h_1^3\right)^2 \left(\mathbb{1} + \overline{h}_1 L_{\vec{\mathbf{x}}}^\dagger + \overline{h}_1^2 L_{\vec{\mathbf{x}}} + \overline{h}_1^3\right)^2 \right\}. \end{aligned}$$

Finally, the above partition function describes a system of static quarks converging to full QCD with the limit $\kappa \to 0$, which is the infinite quark mass limit.

3.4 Kinetic Quark Determinant to leading order

After we have discussed the static determinant in detail, the next major step is to calculate the kinetic determinant. We set the starting point at Eq. (3.18) and take a closer look at the right term:

$$\det Q_{\text{kin}} = \det\left[\mathbb{1} - \frac{\kappa S}{\mathbb{1} - \kappa T}\right] \tag{3.24}$$

$$= \det\left[\mathbb{1} - \frac{\kappa(S^+ + S^-)}{1 - \kappa\, T}\right] = \det\left[\mathbb{1} - \frac{\kappa\, S^+}{Q_{\text{stat}}} - \frac{\kappa\, S^-}{Q_{\text{stat}}}\right] \tag{3.25}$$

$$= \exp \operatorname{Tr} \log\left[1 - (P + M)\right] = \exp \operatorname{Tr}\left[-\sum_{n=1}^{\infty} \frac{1}{n}(P + M)^n\right] \tag{3.26}$$

$$= \exp\left[-\sum_i \operatorname{Tr} P_i M_i + \mathcal{O}(\kappa^4)\right] \tag{3.27}$$

Here the static propagator is defined as

$$Q_{\text{stat}}^{-1} = \left[1 - \kappa\, T\right]^{-1} \tag{3.28}$$

and in addition to that the two quantities $P \equiv \frac{\kappa\, S^+}{Q_{\text{stat}}}$ and $M = \frac{\kappa\, S^-}{Q_{\text{stat}}}$ have been defined. Moreover the identity in Eq. (3.13) and the series expansion of the logarithm was used again. After expanding in leading order, the definitions for P, M were put back in place. In the last step, the same argumentation as in section 3.3 was used. Note that in the following the order $\mathcal{O}(\kappa^4)$ will be omitted. In Appendix A.3 the static propagator from Eq. (3.28) was explicitly calculated and has the form

$$Q_{x,y}^{-1} = A_{x,y}^+ + A_{x,y}^- + \gamma_0\big(B_{x,y}^+ - B_{x,y}^-\big) \equiv A_{x,y} + \gamma_0 B_{x,y} \tag{3.29}$$

where $A^\pm$ and $B^\pm$ are expressions to summarize various terms. For deeper understanding see Appendix A.3 and especially Eq. (A.29). Now that we have explicitly calculated the static propagator, we will continue with the kinetic determinant from Eq. (3.27). We reinsert the definitions for the quantities P and M:

$$\det Q_{\text{kin}} = \exp\left[-\kappa^2 \sum_{x,y,i} \operatorname{Tr}\left\{\frac{S_{x,y+i}^+}{Q_{\text{stat}}} \frac{S_{x+i,y}^-}{Q_{\text{stat}}}\right\}\right]$$

$$= \exp\left[-\kappa^2 \sum_{x,y,i} \operatorname{Tr}\left\{S_{x,y+i}^+ (Q_{\text{stat}})^{-1} S_{x+i,y}^- (Q_{\text{stat}})^{-1}\right\}\right]$$

$$= \exp\left[-\kappa^2 \sum_{x,y,i} \operatorname{Tr}\left\{S_{x,y+i}^+ (A_{x,y} + \gamma_0\, B_{x,y})\, S_{x+i,y}^- (A_{x,y} + \gamma_0 B_{x,y})\right\}\right]$$

$$= \exp\left[-\kappa^2 \sum_{x,y,i} \operatorname{Tr}\left\{(A_{x,y} + \gamma_0\, B_{x,y})(1 + \gamma_i)\, U_i(y) (A_{x+i,y+i} + \gamma_0 B_{x+i,y+i})(1 - \gamma_i)\, U^\dagger(x)\right\}\right]$$

In the last step, the definitions for $S^{\pm}_{x,y}$ were inserted. Next: First multiply out the whole term and then calculate the γ matrices at the end. The only term, which will survive is the following

$$\det Q_{\text{kin}} = \exp\left[-4\kappa^2 \sum_{x,y,i} \text{Tr}\left\{B_{x,y}\, U_i(y)\, B_{x+i,y+i}\, U^\dagger(x)\right\}\right]. \tag{3.30}$$

Next, we can assume that we are on a single site link, which is why $x = y$. Then we get the final result for the kinetic determinant:

$$\det Q_{\text{kin}} = \exp\left[-4\kappa^2 \sum_{x,i} \text{Tr}\left\{B_{x,x}\, U_i(x)\, B_{x+i,x+i}\, U^\dagger(x)\right\}\right]. \tag{3.31}$$

Now that an expression for the kinetic determinant has finally been found, the next step is to perform the spatial integration based on the path integral in Eq. (3.7). For this reason we have to look at:

$$\begin{aligned}
\int [\mathrm{d}U_i] \det Q_{\text{kin}} &= \int [\mathrm{d}U_i] \exp\left[-4\kappa^2 \sum_{x,i} \text{Tr}\left\{B_{x,x}\, U_i(x)\, B_{x+i,x+i}\, U^\dagger(x)\right\}\right] \\
&\approx \int [\mathrm{d}U_i] \left[1 - 4\kappa^2 \sum_{x,i} \text{Tr}\left\{B_{x,x}\, U_i(x)\, B_{x+i,x+i}\, U^\dagger(x)\right\}\right] \\
&= 1 - 4\kappa^2 \sum_{x,i} \int [\mathrm{d}U_i]\, \text{Tr}\left\{B_{x,x}\, U_i(x)\, B_{x+i,x+i}\, U^\dagger(x)\right\}
\end{aligned}$$

In the second step we used the Taylor-Expansion to get rid of the exponential function. The link variables, which are colored in blue in the above equation, will be calculated with the group integral $\int \mathrm{d}U\, U_{ij}\, U^\dagger_{kl} = \frac{1}{N_c}\, \delta_{il}\delta_{jk}$ (see Ref. [36] for more information). It follows

$$\begin{aligned}
\implies \int [\mathrm{d}U_i] \det Q_{\text{kin}} &= 1 - \frac{4\kappa^2}{N_c} \sum_{x,i} \text{Tr}\left\{B_{x,x}\, B_{x+i,x+i}\right\} \\
&= 1 - \underbrace{\frac{4\kappa^2}{N_c}}_{\equiv h_2} \sum_{x,i} \left[\text{Tr}\left\{B^+_{x,x} - B^-_{x,x}\right\} \text{Tr}\left\{B^+_{x+i,x+i} - B^-_{x+i,x+i}\right\}\right]
\end{aligned}$$

where we first defined the nearest neighbor coupling $h_2(\kappa, N_\tau) \equiv \frac{\kappa^2 N_\tau}{N_c}$ and we reinserted the expressions for $B_{x,x}$ from the Appendix A.12. The next step is to insert the expressions for $B^{\pm}_{x,x}$ (cf. Eq. (A.27)), so we finally get the result

$$\begin{aligned}
\int [\mathrm{d}U_i] \det Q_{\text{kin}} = 1 - h_2 \sum_{\vec{\mathbf{x}},i} \Bigg[&\text{Tr}\left(\frac{h_1\, W_{\vec{\mathbf{x}}}}{\mathbb{1} + h_1 W_{\vec{\mathbf{x}}}}\right) - \text{Tr}\left(\frac{\overline{h}_1\, W^\dagger_{\vec{\mathbf{x}}}}{\mathbb{1} + \overline{h}_1 W^\dagger_{\vec{\mathbf{x}}}}\right) \\
&\times \text{Tr}\left(\frac{h_1\, W_{\vec{\mathbf{x}}+i}}{\mathbb{1} + h_1 W_{\vec{\mathbf{x}}+i}}\right) - \text{Tr}\left(\frac{\overline{h}_1\, W^\dagger_{\vec{\mathbf{x}}+i}}{\mathbb{1} + \overline{h}_1 W^\dagger_{\vec{\mathbf{x}}+i}}\right)\Bigg].
\end{aligned} \tag{3.32}$$

From this equation it can be seen that in the leading order a nearest neighbor interaction dominates. Physically, this means that this relation can arise between two quarks, where one can list two anti-quarks or one quark and one anti-quark as examples. Furthermore, we can also state that, as in the static case, there are no temporal dependencies on the coordinates.

Since for the further proceeding it is important that all our terms are expressible by Polyakov loops, we note here that the terms $\mathrm{Tr}\,\frac{h_1 W}{\mathbb{1}+h_1 W}$ and $\mathrm{Tr}\,\frac{\bar{h}_1 W^\dagger}{\mathbb{1}+\bar{h}_1 W^\dagger}$ from the above equation, can be expressed with Polyakov-Loops (see Appendix A.4 for more details).

Chapter 4

Analytic Treatment of the Effective Theory

After the derivation of the effective theory in the last chapter, where our main results were the pure gauge action (cf. Eq. (4.8)), the static determinant (cf. Eq. (3.21)) and the kinetic determinant in leading order (cf. Eq. (3.32)). All these results can be inserted into the partition function, which was mentioned in Eq. (3.5), because in the end only the whole results have to be inserted into the effective action. It follows

$$\begin{aligned}\mathcal{Z} = \int \mathrm{d}L \underbrace{\prod_{\langle \vec{\mathbf{x}},\vec{\mathbf{y}}\rangle} \log\left[1+\lambda_1\left(L^\star_{\vec{\mathbf{x}}}L_{\vec{\mathbf{y}}}+L_{\vec{\mathbf{x}}}L^\star_{\vec{\mathbf{y}}}\right)\right]}_{\textit{pure gauge}} \\ \underbrace{\times \prod_{\vec{\mathbf{x}}}\left(1+h_1L_{\vec{\mathbf{x}}}+h_1^2L^\dagger_{\vec{\mathbf{x}}}+h_1^3\right)^2\left(1+\overline{h}_1L^\dagger_{\vec{\mathbf{x}}}+\overline{h}_1^2L_{\vec{\mathbf{x}}}+\overline{h}_1^3\right)^2}_{\textit{static}} \\ \underbrace{\times \prod_{\langle \vec{\mathbf{x}},\vec{\mathbf{y}}\rangle}\left(\mathbb{1}-h_2\left[\mathrm{Tr}\,\frac{h_1W_{\vec{\mathbf{x}}}}{\mathbb{1}+h_1W_{\vec{\mathbf{x}}}}-\mathrm{Tr}\,\frac{h_1W_{\vec{\mathbf{y}}}}{\mathbb{1}+h_1W_{\vec{\mathbf{y}}}}\right]\right)\left(\mathbb{1}-h_2\left[\mathrm{Tr}\,\frac{\overline{h}_1W^\dagger_{\vec{\mathbf{x}}}}{\mathbb{1}+\overline{h}_1W^\dagger_{\vec{\mathbf{x}}}}-\mathrm{Tr}\,\frac{\overline{h}_1W^\dagger_{\vec{\mathbf{y}}}}{\mathbb{1}+\overline{h}_1W^\dagger_{\vec{\mathbf{y}}}}\right]\right)}_{\textit{kinetic}}.\end{aligned} \tag{4.1}$$

In this equation, the first line is the pure gauge action, the second line is the static determinant, and the last line is the leading order of the kinetic determinant. This partition function has a weak sign problem and can be simulated with different methods: Hence, it is possible to rely, on re-weighting techniques or complex Langevin methods and since the effective couplings correspond to power series of the expansion parameters, they are themselves small in the range of plausibility. Hence, the effective theory can also be treated as a linked-cluster expansion method known from statistical physics, with results for thermodynamic observables. An important insight here is that the original sign problem is under control and we have an explicit expression to determine other important physical properties [37].

One common feature that all of these results share is that they were all finally expressed in terms of Polyakov loops. This is vastly important, because the basic assumption was that we were looking at an effective theory, which of course describes real physics. In doing so, we know that the Polyakov loop is a

suitable order parameter, because its deconfinement and symmetry properties fit it well. Either way, the goal of this chapter is to motivate the mean field approach, where this approach is done for the Polyakov loop. Thereby for the Polyakov-Loop the approach $L_{\vec{x}} = \overline{L}_{\vec{x}} + \delta L_{\vec{x}}$ and $L^{\star}_{\vec{x}} = \overline{L}_{\vec{x}} + \delta L^{\star}_{\vec{x}}$ will be used.

4.1 Mean Field Theory

Mean field theory is a method used in statistical physics. The basic idea of this theory is that instead of evaluating the entire microscopic theory, one approximates the interactions in the theory by a mean field, which is usually the order parameter of the statistical system. This is much easier to evaluate and also provides an analytical approach to the theory. Mean-field theory is a good choice because since only a few lattice models can be solved explicitly, one is interested in efficient approximation methods. A simple and universal approximation is the mean-field approximation, which gives qualitatively correct results for many lattice systems [38].

4.1.1 Deriving a formula for Mean Field Free Energy

To begin with, we start with the mean field ansatz, which looks like

$$\mathcal{F}_{\text{mf}} = \mathcal{F}_{\text{ss}} + \overline{\mathcal{F}} \tag{4.2}$$

where the single site free energy is denoted with $\mathcal{F}_{\text{ss}} = -\log(\mathcal{Z}_{ss})$. The mean field energy is therefore composed of the single site free energy and a mean field. Here, $\overline{\mathcal{F}}$ is not known and is calculated in the context by minimizing the entire equation according to $\frac{\partial \mathcal{F}_{\text{mf}}}{\partial \overline{L}} \overset{!}{=} 0$. Accordingly, the whole Eq. (4.2) is now derived after the mean field

$$\frac{\partial \mathcal{F}_{\text{mf}}}{\partial \overline{L}} = \frac{\partial \mathcal{F}_{\text{ss}}}{\partial \overline{L}} + \frac{\partial \overline{\mathcal{F}}}{\partial \overline{L}}.$$

Since $\overline{\mathcal{F}}$ is not known here and will be calculated later, we start the calculation by first calculating the emerging blue term, which follows after a short calculation

$$\begin{aligned} \frac{\partial \mathcal{F}_{\text{ss}}}{\partial \overline{L}} &= -\frac{\partial}{\partial \overline{L}} \ln(\mathcal{Z}_{\text{ss}}) \\ &= -\frac{1}{\mathcal{Z}_{\text{ss}}} \frac{\partial}{\partial \overline{L}} \mathcal{Z}_{\text{ss}} \\ &= -\frac{1}{\mathcal{Z}_{\text{ss}}} \int \mathrm{d}L \exp\left\{ \frac{\partial S^{\text{eff}}}{\partial \overline{L}} L - \frac{\partial S^{\text{eff}}}{\partial \overline{L^{\star}}} L^{\star} \right\} \left[\frac{\partial^2 S^{\text{eff}}}{\partial \overline{L}^2} L - \frac{\partial^2 S^{\text{eff}}}{\partial \overline{L} \partial \overline{L^{\star}}} L^{\star} \right], \end{aligned} \tag{4.3}$$

where the partition function takes the form

$$\mathcal{Z}_{ss} = \int \mathrm{d}L \exp\left\{ \frac{\partial S^{\text{eff}}}{\partial \overline{L}} L - \frac{\partial S^{\text{eff}}}{\partial \overline{L^{\star}}} L^{\star} \right\}. \tag{4.4}$$

Here, S^{eff} refers to the effective action, which is later implemented by the effective theory, which was derived in the last chapter.

The result for the blue term calculated above in Eq. (4.3) is inserted back into the mean field ansatz. Therefore it follows

$$0 \overset{!}{=} \frac{\partial \mathcal{F}_{\text{mf}}}{\partial \overline{L}} \tag{4.5}$$

$$= -\frac{1}{\mathcal{Z}_{\text{ss}}} \int \mathrm{d}L \exp\left\{ \frac{\partial S^{\text{eff}}}{\partial \overline{L}} L - \frac{\partial S^{\text{eff}}}{\partial \overline{L}^\star} L^\star \right\} \left[\frac{\partial^2 S^{\text{eff}}}{\partial \overline{L} \partial \overline{L}^\star} L - \frac{\partial^2 S^{\text{eff}}}{\partial \overline{L} \partial \overline{L}^\star} L^\star \right] + \frac{\partial \overline{\mathcal{F}}}{\partial \overline{L}}. \tag{4.6}$$

Reordering this expression leads to

$$\begin{aligned}
\frac{\partial \overline{\mathcal{F}}}{\partial \overline{L}} =& - \frac{\partial^2 S^{\text{eff}}}{\partial \overline{L}^2} \underbrace{\frac{1}{\mathcal{Z}_{\text{ss}}} \int \mathrm{d}L \exp\left\{ \frac{\partial S^{\text{eff}}}{\partial \overline{L}} L - \frac{\partial S^{\text{eff}}}{\partial \overline{L}^\star} L^\star \right\} L}_{\langle L \rangle \equiv \overline{L}} \\
& - \frac{\partial^2 S^{\text{eff}} L}{\partial \overline{L} \partial \overline{L}^\star} \underbrace{\frac{1}{\mathcal{Z}_{\text{ss}}} \int \mathrm{d}L \exp\left\{ \frac{\partial S^{\text{eff}}}{\partial \overline{L}} L - \frac{\partial S^{\text{eff}}}{\partial \overline{L}^\star} L^\star \right\} L^\star}_{\langle L^\star \rangle \equiv \overline{L}^\star} \\
=& \frac{\partial^2 S^{\text{eff}}}{\partial \overline{L}^2} \overline{L} - \frac{\partial^2 S^{\text{eff}} L}{\partial \overline{L} \partial \overline{L}^\star} \overline{L}^\star \\
=& - \left[\frac{\partial}{\partial \overline{L}} \left(\frac{\partial S^{\text{eff}}}{\partial \overline{L}} \right) - \frac{\partial S^{\text{eff}}}{\partial \overline{L}} \right] - \frac{\partial^2 S^{\text{eff}}}{\partial \overline{L} \partial \overline{L}^\star} \overline{L}^\star \\
=& - \frac{\partial}{\partial \overline{L}} \left(\frac{\partial S^{\text{eff}}}{\partial \overline{L}} \right) + \frac{\partial S^{\text{eff}}}{\partial \overline{L}} - \frac{\partial^2 S^{\text{eff}}}{\partial \overline{L} \partial \overline{L}^\star} \overline{L}^\star .
\end{aligned}$$

We can state that the identities of the expected values of the Polyakov-Loops are written in the formula in which we also have the expected value of the Polyakov-Loops. The claim is here that the expected values of the Polyakov-Loop are the same as the values of the mean field, because the mean field approach satisfies the so called self-consistency equation. This assumption is justified by the fact that no Polyakov-Loop is unique and its expected value should be the same as the mean field value of the surrounding spins.

Furthermore, in the further process of the calculation, the inverse product rule was used and in the last step, the complete equation was integrated out according to $\overline{L}$. This leads to the final result

$$\Rightarrow \boxed{\overline{\mathcal{F}} = -\frac{\partial S^{\text{eff}}}{\partial \overline{L}} \overline{L} - \frac{\partial S^{\text{eff}}}{\partial \overline{L}^\star} + S^{\text{eff}}}. \tag{4.7}$$

This equation provides an expression for the mean free field energy and can be easily calculated if the effective action is known. For the continuation, this effective action is known and adopted by the effective theory, where the results for the effective action are all encoded in Eq. (4.1).

4.2 Result: Pure Gauge Theory

After the derivation of the mean field formula in the last section, the next step is to apply this formula to the pure gauge case. The aim of this chapter is to show an example calculation with mean field, because the calculations are straightforward and the same procedure has been used for other considerations. First we will integrate the Polyakov-Loops and the associated mean field ansatz into the pure gauge action and then, using the formula derived in Eq. (4.7), the mean field free energy is calculated.

The aim of this section is to show an example calculation with mean field, because the calculations are straightforward and the same procedure has been used for other cases such as for the static and kinetic determinant. Since the calculations for the static and kinetic determinant are very sprawling to show, therefore, the calculation is discussed here in particular in order to have a better understanding of the mean field approach.

For this reason we start with the pure gauge action (cf. Eq. (3.12)) and integrate the mean field approach into the theory:

$$
\begin{aligned}
S_{\text{p.g.,NN}} &= \sum_{\vec{\mathbf{x}}} S\left(L_{\vec{\mathbf{x}}}, L_{\vec{\mathbf{x}}}^{\dagger}\right) = -\sum_{\vec{\mathbf{x}}}\sum_{i=1}^{d} \log\left[1+\lambda_1\left(L_{\vec{\mathbf{x}}}L_{\vec{\mathbf{x}}+i}^{\dagger}+L_{\vec{\mathbf{x}}}^{\dagger}L_{\vec{\mathbf{x}}+i}\right)\right] \qquad (4.8)\\
&= -\sum_{\vec{\mathbf{x}}}\sum_{i=1}^{d} \log\left[1+\left\{\left(\overline{L}_{\vec{\mathbf{x}}}+\delta L_{\vec{\mathbf{x}}}\right)\left(\overline{L}_{\vec{\mathbf{x}}+i}^{\star}+\delta L_{\vec{\mathbf{x}}+i}^{\star}\right)+\left(\overline{L}_{\vec{\mathbf{x}}}^{\star}+\delta L_{\vec{\mathbf{x}}}^{\star}\right)\left(\overline{L}_{\vec{\mathbf{x}}+i}+\delta L_{\vec{\mathbf{x}}+i}\right)\right\}\right]\\
&= -\sum_{\vec{\mathbf{x}}}\sum_{i=1}^{d} \log\left[1+\lambda_1\left(\overline{L}_{\vec{\mathbf{x}}}\,\overline{L}_{\vec{\mathbf{x}}+i}^{\star}+\overline{L}_{\vec{\mathbf{x}}}^{\star}\,\overline{L}_{\vec{\mathbf{x}}+i}\right)\right]\\
&\approx -d\sum_{\vec{\mathbf{x}}} \log\left[1+2\lambda_1\overline{L}_{\vec{\mathbf{x}}}\,\overline{L}_{\vec{\mathbf{x}}}^{\star}\right]\\
&= -d\sum_{\vec{\mathbf{x}}} \log\left[1+2\lambda_1\left|\overline{L}_{\vec{\mathbf{x}}}\right|^2\right]
\end{aligned}
$$

Here we used the mean field approach for the Polyakov-Loop $L_{\vec{\mathbf{x}},i} = \overline{L}_{\vec{\mathbf{x}}}+\delta L_{\vec{\mathbf{x}},i}$ and for the $L_{\vec{\mathbf{x}},i}^{\star} = \overline{L}_{\vec{\mathbf{x}}}+\delta L_{\vec{\mathbf{x}},i}^{\star}$ as well. Furthermore we used the periodicity $\vec{\mathbf{x}} \to \vec{\mathbf{x}}+i$ for the nearest neighbor interaction.

Now that we have calculated the pure gauge action (cf. Eq. (4.8)), the next step is to calculate the mean field free energy with use of Eq. (4.7).

$$
\begin{aligned}
\overline{\mathcal{F}} &= \frac{\partial S_{\text{p.g.,NN}}}{\partial \overline{L}}\overline{L} - \frac{\partial S_{\text{p.g.,NN}}}{\partial \overline{L}^{\star}}\overline{L}^{\star} + S_{\text{p.g.,NN}}\\
&= \frac{4\lambda_1 d\left|\overline{L}\right|^2}{1+2\lambda_1\left|\overline{L}\right|^2} - d\log\left[1+2\lambda_1\left|\overline{L}\right|^2\right]\\
&= \frac{2d\left(2\lambda_1\left|\overline{L}\right|^2+1-1\right)}{1+2\lambda_1\left|\overline{L}\right|^2} - d\log\left[1+2\lambda_1\left|\overline{L}\right|^2\right]\\
&= \frac{2d\cancel{\left(2\lambda_1\left|\overline{L}\right|^2+1\right)}}{\cancel{1+2\lambda_1\left|\overline{L}\right|^2}} - \frac{2d}{1+2\lambda_1\left|\overline{L}\right|^2} - d\log\left[1+2\lambda_1\left|\overline{L}\right|^2\right]
\end{aligned}
$$

Finally it follows

$$\Longrightarrow \quad \overline{\mathcal{F}} = -2d\left[-1 + \frac{1}{1+2\lambda_1\left|\overline{L}\right|^2} + \frac{1}{2}\log\left(1+2\lambda_1\left|\overline{L}\right|^2\right)\right]. \tag{4.9}$$

The only missing part is the single site free energy, which is computed via the partition function (cf. Eq. (4.4)). So we get

$$\begin{aligned}
\mathcal{Z}_{\text{ss}} &= \int \mathrm{d}L\ \exp\left[-\frac{\partial S}{\partial \overline{L}}L - \frac{\partial S}{\partial \overline{L}^\star}L^\star\right] \\
&= \int \mathrm{d}L\ \exp\left[\frac{\partial}{\partial \overline{L}}\left[-d\log 1 + 2\lambda_1\left|\overline{L}\right|^2\right]L - \frac{\partial}{\partial \overline{L}^\star}\left[-d\log 1 + 2\lambda_1\left|\overline{L}\right|^2\right]L^\star\right] \\
&= \int \mathrm{d}L\ \exp\left[\underbrace{\frac{2d\lambda_1\overline{L}^\star}{1+2\lambda_1\left|\overline{L}\right|^2}}_{\equiv z_1}L + \underbrace{\frac{2d\lambda_1\overline{L}}{1+2\lambda_1\left|\overline{L}\right|^2}}_{\equiv z_2}L^\star\right] \\
&= \sum_{n=0}^{\infty}\sum_{m=0}^{\infty}\frac{z_1^n}{n!}\frac{z_2^m}{m!}\underbrace{\int \mathrm{d}L\ L^n(L^\star)^m}_{\equiv \mathcal{I}(n,m)}.
\end{aligned}$$

Here the series expansion of the exponential function was used. The integrals appearing in expression $\mathcal{I}(n,m)$ are calculated as in Appendix A.5 explained. In particular, the derived Eq. (A.39) will be a calculation rule for the Polyakov-Loop integrals. At this point it should be mentioned again that the integrals in $\mathcal{I}(n,m)$ always give a natural number as a contribution. Finally for the single site free energy it follows

$$\mathcal{F}_{\text{ss}} = -\log\left[\sum_{n=0}^{\infty}\sum_{m=0}^{\infty}\frac{z_1^n}{n!}\frac{z_2^m}{m!}\mathcal{I}(n,m)\right]. \tag{4.10}$$

Now that all parts of the mean field free energy $\mathcal{F}_{\text{mf}} = \mathcal{F}_{\text{ss}} + \overline{\mathcal{F}}$ have been calculated (cf. Eq. (4.9) and Eq. (4.10)), the next step is to plot these quantities and to analyze them.

The first order nature of the transition is exhibited in Fig. 4.1, where the mean field free energy is plotted against the real part of Polyakov-Loop. The behavior of the free energy with pure gauge action shows that the figure contains two degenerate minima (one in the origin and the other at $\langle L\rangle \approx 0.6$) for the critical value of $\lambda_{\text{c}} \sim 0.152$. We can observe here that for different λ a first order phase transition occurs, because the symmetry breaks spontaneously for a certain critical value of the coupling λ. The background to this symmetry breaking lies in the fact that Polyakov-Loop has three different sectors in the high temperature area, which is closely related to the coupling λ. To be even more precise: We know that in leading order the effective coupling λ is something like $\lambda \approx u(\beta)^{N_\tau}$, where $u(\beta)$ is the fundamental character expansion coefficient and β is the inverse coupling [34]. We also know that $T = \frac{1}{aN_\tau}$, so we can

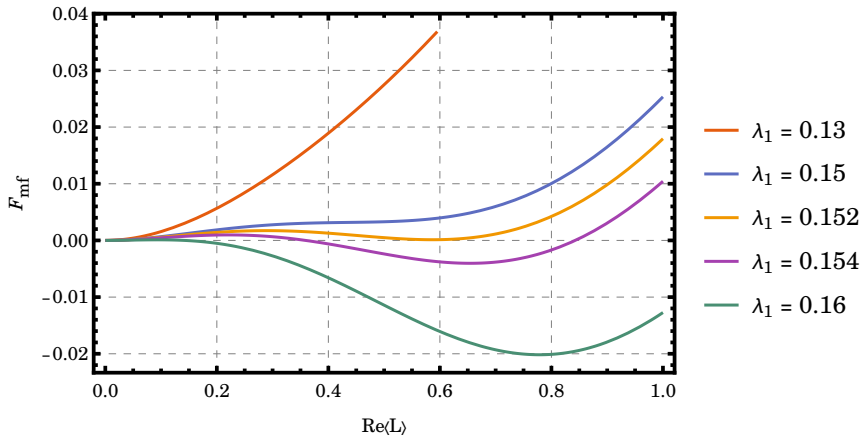

Figure 4.1: Mean-Field free energy $\mathcal{F}_{mf}$ as a function of the expectation value of the Polyalov-Loop $\langle L \rangle$, with different values around the critical values of λ_1.

conclude that when λ is increased automatically the temperature of the system is also increased and the Polyakov-Loop is not anymore in the disordered phase. In other words: The Polyakov-Loop will be non-zero anymore and this is exactly the situation where the phase transition occurs. It is also well known that the Polyakov loop is related to the exponential of the free energy F_q of a static quark, connecting the expectation value of the Polyakov loop $\langle L \rangle$ to the confinement and deconfinement properties of QCD [39].

To compare with: In Ref. [40] the authors used a series expansion, which leads to a critical value of $\lambda_c = 0.14$. Furthermore in Ref. [41] the authors used a quite similar approach with the spin model and they get a critical value for $\lambda_c = 0.134$. We can conclude that our approach has a deviation by $(7.7 \sim 10.1)\%$.

4.3 Result for $N_f = 1$: Static Determinant

In the previous section we studied the pure gauge case, where we considered the pure gauge action with no quarks at all. We know from the calculation in Sec. 3.2 that the fermionic contribution comes along with the hopping expansion of the Wilson-Dirac-Operator, or to be more precise with the effective coupling for quarks $h_1 = e^{N_\tau(a\mu+\ln 2\kappa)}$ and anti-quarks $\overline{h}_1 = e^{N_\tau(-a\mu+\ln 2\kappa)}$, where the masses of the fermions are encoded in $\kappa \propto \frac{1}{m_{\text{quark}}}$.

However this is the reason why we extend our study of the effective theory by including the static quark action as well, which is also part of the Eq. (4.1). It is important to mention that the kinetic determinant is set to one, i.e. $\det Q_{kin} = 1$, because this implies that infinitely heavy quarks become interesting for the following process. Furthermore, our special interest is that there must be only hops in the temporal direction. Beyond that only hops in temporal direction are allowed, because we are dealing only with the single-site action S_{ss} and the static determinant.

The following strategy is intended for the subsequent process: We study the effective theory for the $\mu = 0$ case, which in turn implies that $h_1 = \overline{h}_1$. This is due to the fact how h_1 and $\overline{h}_1$ are defined, because all terms are the same, except for the chemical potential part (cf. Eq. (3.22)). Further this signifies that the effective theory with the static determinant has only two free parameters, which are in this case h_1 and λ_1. In the pure gauge case we observed that a phase transition occurs when the effective gauge coupling λ_1 was increased and this corresponds to the deconfinemnet transition. The question is will this connection also take place with the static determinant, when the efffective quark coupling is also present. To verify this, the same procedure for the Mean Field as in the last section will be used next. Here, only the static determinate appears as an additional expression, whereby the mean field approach of Eq. (4.2) is also applied here.

Fig. 4.2 demonstrates the Mean Field free energy F_{mf} as a function of the expectation value of the Polyakov-Loop $\langle L \rangle$ with the effective quark and as well the gauge coupling. The mean field free energy is studied in a way that the previous degeneracy of the minima will be investigated. However the way to do this is to increase κ which automatically implies that $h_1 \sim e^{\ln(2\kappa)} \sim \kappa$ and because of $\kappa \propto 1/m_q$ this will corresponds to lowering the masses of the quarks.

In the mentioned Fig. 4.2 we can observe that for increasing h_1 and lowering gauge coupling λ_1 we observe a first order phase transition. Especially at $h_1 = 0.004$ and $\lambda = 0.1471$ the system contains two degenerate minima like in the pure gauge case. The symmetry breaks for increasing quark coupling and the phase transition slowly vanishes and transforms itself to a second order phase transition. The results from Fig. 4.2 are in accordance with Ref. [40, 41, 42], which studied the phase transition from a different starting point. The authors used a chiral spin model, which is conceptually simpler in its physical description. We can finally summarize that the Mean Field theory applied on the effective theory gives us results, which are in accordance with the literature and furthermore it showed the direct connection between deconfinement property of QCD.

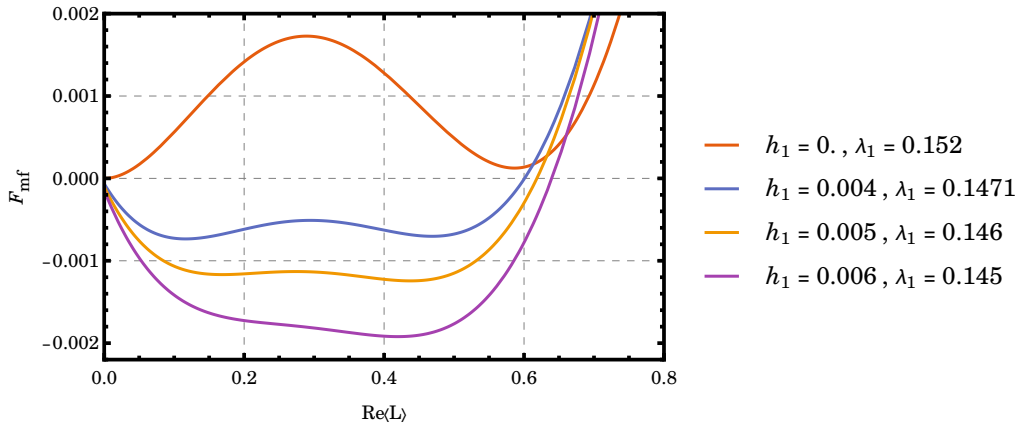

Figure 4.2: Mean-Field free energy $\mathcal{F}_{mf}$ as a function of the expectation value of the Polyalov-Loop $\langle L \rangle$, with different values around the critical values of λ and the effective quark coupling h.

4.4 Results for $N_f = 2$: Adding μ_I and μ_B into the Effective Theory

After applying the mean field theory for pure gauge and the static determinant in the last two sections, it is now time to increase the complete partition function, which is defined in Eq. (4.1). We note again that the procedure for the mean field approach does not change. As in the last sections described, we first compute the action using the mean field approach for the Polyakov-Loops and then finally the other quantities mentioned in Eq. (4.2).

4.4.1 Adding Isospin into the Theory

Apart from our mean field study, the next step is to extend the theory with $N_f = 2$, or to be more precise we will next implement the isospin in the theory. Since the last considerations were for the $N_f = 1$ case, we now have to look at the partition function for multiple flavors. For $N_f = 2$ the partition function from Eq. (3.5) becomes

$$\mathcal{Z} = \int [\mathrm{d}U_0] \det Q_u \ \det Q_d \ e^{-S_g}, \tag{4.11}$$

where each new flavor also introduces a new hopping parameter, which is either κ_u or κ_d. The static partition function becomes then

$$\mathcal{Z} = \int [\mathrm{d}U_0] \prod_{\vec{\mathbf{x}}} \left(1 + h_{1,u} L_{\vec{\mathbf{x}}} + h_{1,u}^2 L_{\vec{\mathbf{x}}}^\star + h_{1,u}^3\right)^2 \left(1 + h_{1,d} L_{\vec{\mathbf{x}}} + h_{1,d}^2 L_{\vec{\mathbf{x}}}^\star + h_{1,d}^3\right)^2. \tag{4.12}$$

Next we will take a closer look to the kinetic determinant

$$\det Q_{\text{kin}} = \det\left[1 - P_u - M_u\right] \det\left[1 - P_u - M_u\right] \tag{4.13}$$

$$= \exp\left[\text{Tr}\sum_{n=1}^{\infty}\left[-\frac{1}{n}(P_u + M_u)^n\right] + \text{Tr}\sum_{n=1}^{\infty}\left[-\frac{1}{n}(P_d + M_d)^n\right]\right]. \tag{4.14}$$

For degenerate quarks, thus $\kappa_d = \kappa_u$, the kinetic quark determinant can also be written as

$$Q_{\text{kin}}^{N_f} = \exp\left[N_f \ \text{Tr}\sum_{n=1}^{\infty}\left[-\frac{1}{n}(P + M)^n\right]\right]. \tag{4.15}$$

This case allows that all expressions stay the same, only the factor N_f has been considered. Now that the theory has been verified for multiple flavors, the next step is to introduce isospin. This is described in the literature as $\mu_I = (\mu_u - \mu_d)/2$ after which $\mu_u = -\mu_d$ follows [14]. Accordingly, the only effort was to insert the above defined isospin into the mean field free energy $\mathcal{F}_{\text{mf}}$.

This relationship is described precisely by Fig. 4.3, which contains two plots. In both plots, on the x-axis the real part of the Polyakov-Loop $\langle L \rangle$ is shown, whereas on the y-axis the mean field free energy $\mathcal{F}_{\text{mf}}$ is demonstrated. These simulations were performed with the lattice parameters for $\beta = 5.7$, $N_c = 3$ and $N_\tau = 10000$. With N_τ, we are in the low temperature range, since due to $T \propto \frac{1}{N_\tau}$ this connection remains, whereby the more exact correlation with the temperature will become clearer later in the next section.

The difference between the two plots is due to the fact, which parameter is held, since in the upper plot κ is fixed and isospin chemical potential μ_I is varied, while in the lower plot, the isospin chemical potential μ_I is held and finally κ varied.

Both plots can clearly show that when the lattice parameters μ_I and κ are changed, there is a continuous change for the global minima in the positive direction of the expectation value of the Polyakov-Loop $\langle L \rangle$. This is a clear indicator for the study of phase transitions, because this fact points to a second-order phase transition, because if the order parameter, which is in our case $\langle L \rangle$ slowly changes from zero to a finite value.

Now that the isospin has been inserted, the analysis will be continued in the next section, where the baryonic chemical potential μ_B will be inserted.

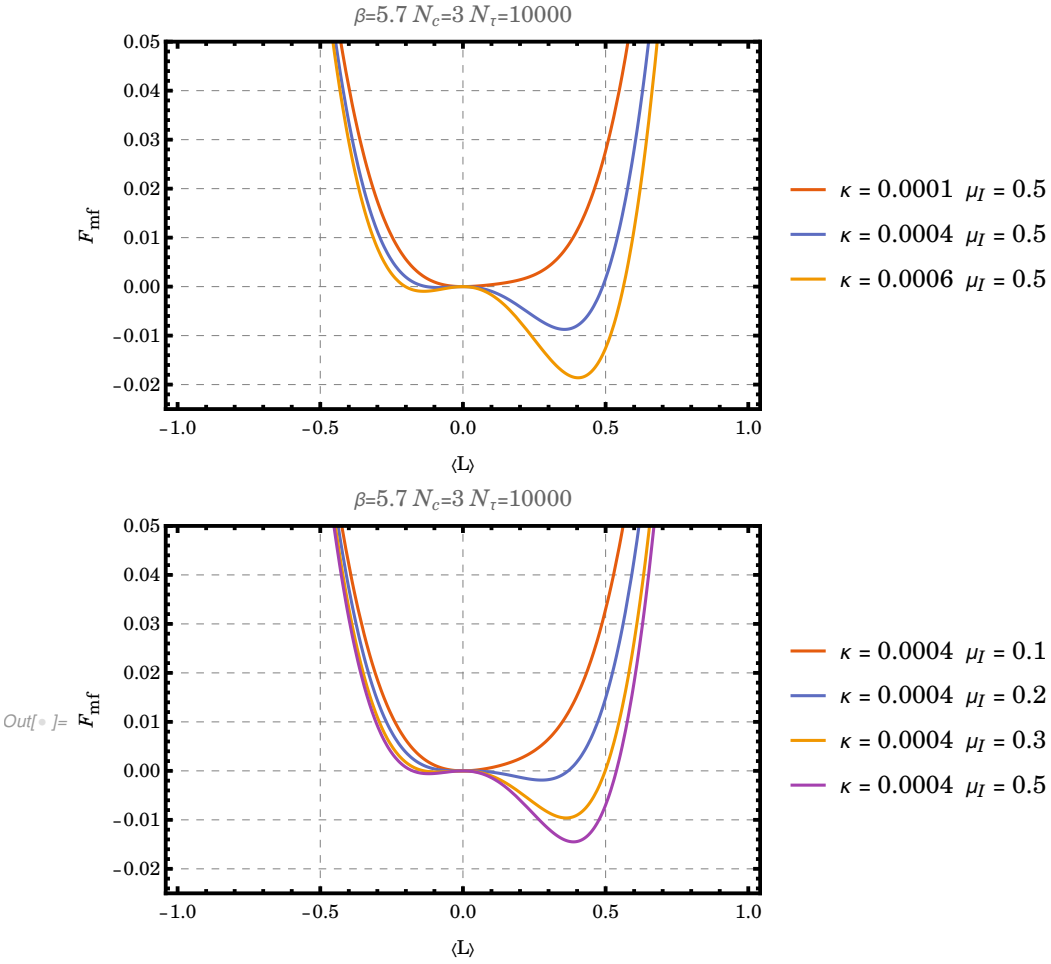

Out[ ]=

Figure 4.3: Mean-Field free energy $\mathcal{F}_{mf}$ as a function of the expectation value of the Polyakov-Loop $\langle L \rangle$ with respect to the isospin chemical potential and different κ. Lattice Parameters: $\beta = 5.7$, $N_c = 3$ and $N_\tau = 10000$.

4.4.2 The (μ_I, μ_B) Phase Diagram

In the last section the mean field free energy with the isospin was considered more exactly, whereby now the theory is extended with the baryonic potential. The lattice parameters remain the same as in the last section, i.e. $\beta = 5.7$, $N_c = 3$ and $N_\tau = 10000$. This concept has been realized in 4.4, where again the real part of the Polyakov-Loop $\langle L \rangle$ is shown on the x-axis and on the y-axis the mean field free energy $\mathcal{F}_{mf}$ is illustrated. In this plot the lattice parameter κ is fixed here and has the value $\kappa = 0.0009$, which corresponds to heavy quarks, because of $\kappa \propto \frac{1}{m_q}$.

The interesting thing about Fig. 4.4 is that a phase transition can also be identified here. More precisely, a first-order phase transition is visible at the combination of $\mu_B = 0.125$ and $\mu_I = 0.3$ (see blue line in Fig. 4.4). Furthermore, a continuum shift of the global minima can be seen, whereby this shift slowly smoothed out for further combinations of μ_I and μ_B. This connection was already clear in the last chapter, where we identify a second order phase transition for the isospin chemical potential. To summarize, this figure shows that two different phase transitions can be observed, which can both be explained as follows: First, the pure phase transition at μ_I is related to a second-order phase transition due to the breaking of isospin symmetry [14]. The first order phase transition at the introduction of the baryonic chemical potential μ_B is explained by the fact that we are at low temperature and locally at the Liquid-Gas transition line in the QCD phase diagram. At least here it is clear that it must be a first order phase transition. The intriguing thing here is that these two findings appear together, so it would be an interesting next step to plot the isospin and baryonic chemical potential quantities as a function of the mean field free energy.

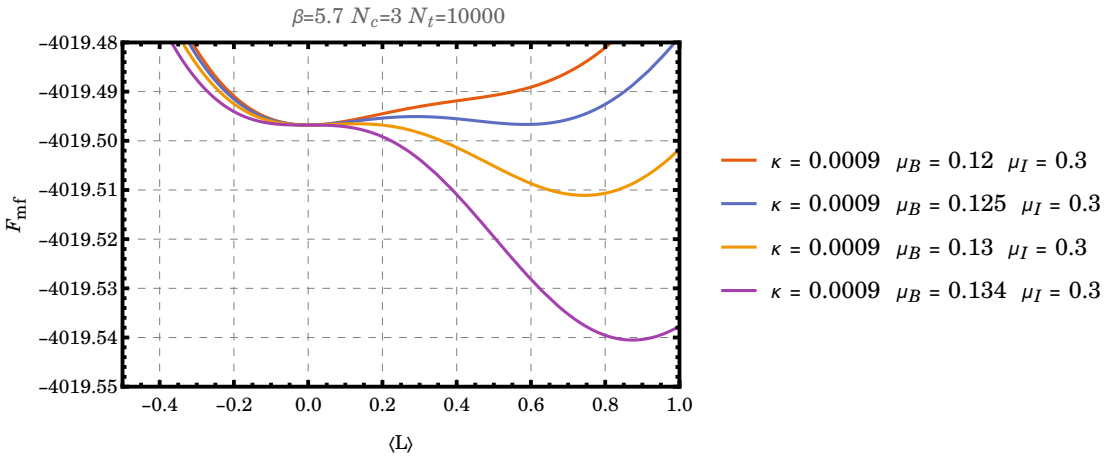

Figure 4.4: Mean-Field free energy $\mathcal{F}_{mf}$ as a function of the expectation value of the Polyakov-Loop $\langle L \rangle$ with respect to the isospin and baryonic chemical potential for a fixed κ. Lattice Parameters: $\beta = 5.7$, $N_c = 3$ and $N_\tau = 10000$

The consideration to map the isospin and baryonic chemical potential with the mean field free energy is illustrated in Fig. 4.5. In this figure the isospin chemical potential is plotted on the x-axis and the baryonic potential on the y-axis, where the lattice parameters, i.e. $\beta = 5.7$, $N_c = 3$ and $N_\tau = 10000$ stay the same. Moreover the temperature and the baryonic chemical potential μ_B were connected over

$$\frac{m_B}{T} = \frac{am_B}{aT} = N_\tau \, am_B = -3N_\tau \log(2\kappa).$$

Here we used $N_\tau = \frac{1}{aT}$ and $am_B = -3\log(2\kappa)$ in leading order. The exact same procedure can also be done with the isospin chemical potential μ_I, where the slight difference is that the pion mass m_π has to be considered. In the effective theory, the pion mass in leading order is denoted as $am_\pi = -2\log(2\kappa)$ [43].

To understand this diagram, it is important to consider the temperature T as the third axis, as it is usually added to the QCD phase structure. And here we will consider two cases: On the one hand, the case when the temperature goes to zero, which indicates that the study will be only valid in the low temperature range and on the other hand, when the temperature is finite.

The former case is easier to explain, because at $T \to 0$ it must be a phase transition, because the symmetry is already broken. This can be explained most simply with a condensate, because if a condensate is available, then there is a medium and accordingly a preferred system. Due to the symmetry breaking, the Lorentz invariance will be broken and this corresponds with a phase transition of first order. This fact, or more precisely this circumstance was also shown in Fig. 4.4, where the combination of the isospin and the baryonic chemical potentials were shown.

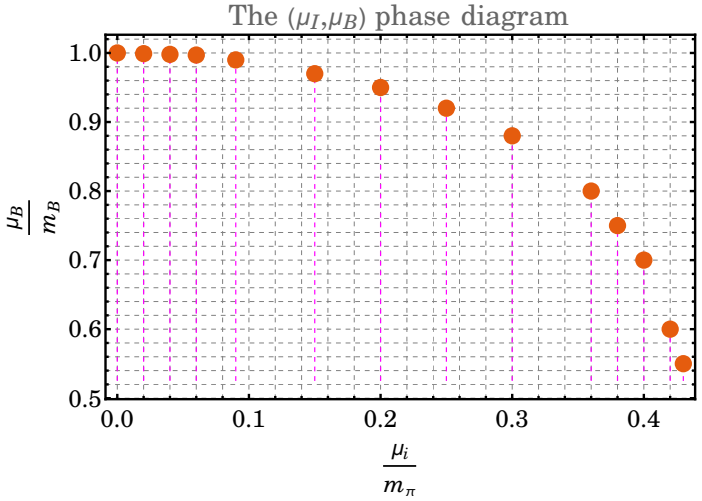

Figure 4.5: Derived phase diagram from the mean field free energy at small temperatures for different combinations of the isospin and baryonic chemical potential. Lattice parameters: $\beta = 5.7$, $N_c = 3$ and $N_\tau = 10000$.

However, the other case at finite temperature, its more complicated to determine the phase transition. At first, it is possible to assume that since the

Liquid-Gas transition has been a second order endpoint, which in turn also means that a second order line exists, all lines converge to a tri-critical endpoint, where exactly the behavior of the curve in Fig. 4.5 takes place. Now, the problem lies lies in the fact of the qualitative shape of the curve in Fig. 4.5, because for finite temperature the curve points not exactly in the same direction, like the well known (μ_I, T) phase diagram plot [14]).

A possible explanation could be that the mean-field theory is only an approximation to the true nature of the QCD phase structure and loses the necessary accuracy in respect for the simplification of assumption, which mean field clearly does. Nevertheless, the fact remains that the mean field theory is usually a good approach and provides basically correct results, as we have seen from our previous results. A hypothesis that could also be put forward would be the possibility to analyze in more detail the phase structure of the QCD in the upper area of the (μ_I, T) plot, whereby the possibility that no longer second-order line exists can be considered. Therefore the qualitative shape of Fig. 4.5 could give a possible course of the behavior. However, further research is being conducted in this direction.

Chapter 5

Conclusion and Outlook

In this thesis, a three dimensional effective theory for Lattice-QCD was derived by a strong coupling and hopping expansion in the heavy quark regime, where the final path integral and its components have been treated analytically via a mean field approximation. This approach was quite promising because mean field theory is often a suitable approximation scheme for lattice systems, which are generally difficult to solve and therefore this technique provides an useful way to get at least qualitative results for the whole theory.

In this thesis mean field was applied for the order parameter $L_{\vec{x}}$ and the free energy $\mathcal{F}$ of the system. Here, it was crucial that every Polyakov-Loop mean field ansatz was correctly added into the prepared action. The kinetic and the static action were evaluated with Mathematica, because in comparison to the pure gauge action, the kinetic and static determinant were quite inflated, if the mean field ansatz for the Polyakov-Loops was inserted (see e.g. Sec. 4.2 for an example calculation). Due to $\mathcal{F} = -\ln \mathcal{Z}$, the free energy and the partition function are connected, why first the partition function was calculated and then the single site free energy. After that, the only remaining quantity was $\overline{\mathcal{F}}$ and the calculation is straightforward done with Eq. (4.7).

The first consideration was the pure gauge case, where we have no fermions at all. The result for this case was a spontaneous symmetry breaking, which corresponds to a first order transition for the critical value of $\lambda_c \approx 0.152$. Subsequently the study was extended for the $N_f = 1$ and $N_f = 2$ case, where especially for the two flavor consideration, the isospin chemical potential μ_I was used. This led to a novel phase diagram for the baryonic and isospin chemical potential, where new insights about the QCD phase structure may be reveled. This phase diagram is still under research, because there are still concerns about the finite temperature case. Further research is being pursued in this direction.

Acknowledgments

At this point I would like to thank Prof. Dr. Owe Philipsen for the opportunity to work on this project and to join his working group. Furthermore, I am grateful for every discussion and everyone who took time for me, whereby I would especially like to thank Christoph Konrad, Jonas Scheunert, Alena Zmarsly, Dr. Jangho Kim and Anh Quang Pham in particular. They were always there when I needed help and assistance, even outside of meetings. Moreover, I would like to thank my long-time friend Tom Reichert, who accompanied me through the whole study time and has always been there when I have needed help in any situation. I'll never forget the legendary coffee breaks and the very full filling conversations. Furthermore I would especially like to take this opportunity to thank my family, who have been a great support for the whole time in every possible way, because I always knew that I could always rely on them. And last but not least, I would like to take this opportunity to thank my almost wife Mounia, who has supported me like no one else and has always stayed by my side. For that and much more, I will always be grateful.

Appendices

Appendix A

Appendix

A.1 Corrections for the effective couplings

In this section, the correction terms for the effective couplings λ_1, h_1, $\overline{h}_1$ and h_2 will be determined. First of all, we define [31]

$$u = a_r(\beta) = \frac{1}{3}\frac{c_3(\beta)}{c_1(\beta)} \tag{A.1}$$

where

$$\begin{aligned} c_3(\beta) =& \frac{1}{6}\beta + \frac{1}{72}\beta^2 + \frac{1}{216}\beta^3 + \frac{5}{10368}\beta^4 + \frac{13}{186624}\beta^5 + \frac{77}{11197440}\beta^6 + \frac{139}{201553920}\beta^7 \\ &+ \frac{19}{322486272}\beta^8 + \frac{23}{4837294080}\beta^9 + \frac{319}{9142485811220}\beta^{10} + \frac{2629}{109709829734400}\beta^{11} \\ &+ \frac{16133}{105321436545024 00}\beta^{12} + \frac{17499}{189578585781043200}\beta^{13} \\ &+ \frac{35531}{6824829088117555200}\beta^{14} + \mathcal{O}(\beta^{15}), \end{aligned} \tag{A.2}$$

and

$$\begin{aligned} c_1(\beta) =& 1 + \frac{1}{36}\beta^2 + \frac{1}{648}\beta^3 + \frac{1}{2592}\beta^4 + \frac{1}{31104}\beta^5 + \frac{13}{3359232}\beta^6 + \frac{11}{33592320}\beta^7 \\ &+ \frac{139}{4837294080}\beta^8 + \frac{19}{8707129344}\beta^9 + \frac{23}{145118822400}\beta^{10} + \frac{29}{2742745743360}\beta^{11} \\ &+ \frac{2629}{3949553870438400}\beta^{12} \\ &+ \frac{1241}{31596430963507200}\beta^{13} + \frac{17499}{79623006028038144 00}\beta^{14} + \mathcal{O}(\beta^{15}). \end{aligned}$$

Since this work concentrates exclusively on the $N_\tau = 2$ case, the only relevant correction for the nearest neighbor correction is

$$\lambda_1(u) = u^{N_\tau} \exp\left[2\left(4u^4 + 12u^5 - 18u^6 - 36u^7 + \frac{219}{2}u^9 + \frac{830517}{5120}u^{10}\right)\right]. \tag{A.3}$$

For higher orders and its corrections we refer to Ref. [34]. For the effective couplings of the fermion interaction, we get the correction terms [44]

$$h_1(\kappa, N_\tau) = \exp\left[N_\tau(a\mu + \log 2\kappa)\right] \times \exp\left[6N_\tau\kappa^2 u(\frac{1-u^{N_\tau-1}}{1-u}4u^4 - 12\kappa^2 + 9\kappa^2 u + 4\kappa^2 u^2 - 4\kappa^4)\right], \tag{A.4}$$

where for the anti-quark coupling $\overline{h}_1$ the same corrections will be applied. Finally the only missing part is the coupling of the $\mathcal{O}(\kappa^2)$ action h_2, which takes the form

$$h_2(\kappa, N_\tau) = \frac{\kappa^2 N_\tau}{N_c}\left[1 + 2\frac{u - u^{N_\tau}}{1-u} + 8u^5 + 16\kappa^3 u^4\right]. \tag{A.5}$$

A.2 Static determinant: Proof of term $\det\left[\mathbb{1} + h_1 W\right]$

$$\det\left(\mathbb{1} + h_1 W\right) = \exp\left[\operatorname{Tr}\log\left(\mathbb{1} + h_1 W\right)\right] \tag{A.6}$$

$$= \exp\left[\operatorname{Tr}\sum_{k=1}^{\infty}\frac{(-1)^{k+1}}{k}h_1^k \operatorname{Tr} W^k\right] \tag{A.7}$$

$$= \prod_{k=1}^{\infty}\exp\left[\frac{(-1)^{k+1}}{k}h_1^k \operatorname{Tr} W^k\right] \tag{A.8}$$

$$= \prod_{k=1}^{\infty}\sum_{n=0}^{\infty}\frac{(-1)^{k+1}}{k}h_1^{kn}\left(\operatorname{Tr} W^k\right)^n \tag{A.9}$$

First of all, the identity from Eq. (3.13) was used to rewrite the determinant. In the further course the Mercator Series $\log(1+x) = \sum_k \frac{(-1)^{k+1}}{k}x^k$ was used and finally the series representation of the exponential function.

A.3 Calculation of the static propagator

In this section we will take a closer look to the static propagator, which was mentioned in Eq. (3.29). This calculation was also done in Ref. [45]. We will start

$$Q_{\text{stat}}^{-1} = \left(\mathbb{1} - T\right)^{-1} \tag{A.10}$$

$$= \sum_{j=0}^{\infty} T^j \tag{A.11}$$

$$= \mathbb{1} + \sum_{j=1}^{\infty}\left[\left(T^+\right)^j + \left(T^-\right)^j\right], \tag{A.12}$$

where we used the geometric series in the second step. At the end we have inserted the temporal hops from Eq. (3.17). Before we go any further, let's take a closer look at $T^{\pm}$ and rewrite the terms in a different way

$$T^{\pm}(x,y) = z_{\pm}\, P_{\pm}\, U_{\pm}(\vec{\mathbf{x}}, t_x)\, \delta_{t_{\vec{\mathbf{x}}}, t_{\vec{\mathbf{y}}-1}}\, \delta_{\vec{\mathbf{x}},\vec{\mathbf{y}}}\, b^{\mp}_{t_y}. \tag{A.13}$$

Where we have used shorter notations for

$$z_{\pm} = 2e^{\pm a\mu} \;\;,\;\; P_{\pm} = \frac{1}{2}(\mathbb{1} \pm \gamma_0) \;\;,\;\; U_{+0}(\vec{\mathbf{x}}, t_x) = U_0(x) \;\;,\;\; U_{-0}(\vec{\mathbf{x}}, t_x) = U_0^{\dagger}(y)$$

$$\text{and } b_t^- = \begin{cases} -1, & t = 0 \\ 1, & t \neq 0 \end{cases} \;\;,\;\; b_t^+ = \begin{cases} -1, & t = N_t - 1 \\ 1, & t \neq N_t - 1 \end{cases} .$$

Next, we consider our considerations only for T^+, since the calculation for T^- is analogous. We continue with Eq. (A.12) and calculate $(T^+)^j$

$$\left(T^+\right)^j = \delta_{t_{\vec{\mathbf{x}}}, t_{\vec{\mathbf{y}}-1}}\, \delta_{\vec{\mathbf{x}},\vec{\mathbf{y}}}\, z_+^j\, P_+^j\, (U_+(\vec{\mathbf{x}}, t_x))^j \left(b^+_{t_y}\right)^j \tag{A.14}$$

$$= \delta_{t_{\vec{\mathbf{x}}}, t_{\vec{\mathbf{y}}-1}}\, \delta_{\vec{\mathbf{x}},\vec{\mathbf{y}}}\, z_+^j\, P_+ \left[\prod_{i=0}^{j-1} U_0(\vec{\mathbf{x}}, t_x + i)\, b^-_{t_y - i}\right]. \tag{A.15}$$

From the first to the second step we have exploited that the operator $(U_+)^j$ is taken j-times with itself and this is equivalent to writing the operator as a product (analogous for b_{t_y}). Furthermore because of the identity $(\mathbb{1} + \gamma_0)^2 = 2(\mathbb{1} + \gamma_0)$, we can easily show that the relation $(P_+)^j \stackrel{!}{=} P_+$ is valid.

To continue, we need to consider Eq. (A.14) for two distinct cases: First for $t_x = t_y$ and then for $t_x \neq t_y$, where the latter case also splits into $t_x > t_y$ and $t_x < t_y$. Note we can always assume that $\vec{\mathbf{x}} = \vec{\mathbf{y}}$, which is exactly the static case.

So we start with the **first case** $t_x = t_y$:

$$\left(T^+\right)^j = \delta_{t_{\vec{\mathbf{x}}}, t_{\vec{\mathbf{y}}-1}}\, \delta_{\vec{\mathbf{x}},\vec{\mathbf{y}}}\, z_+^j\, P_+^j\, (U_+(\vec{\mathbf{x}}, t_x))^j \left(b^+_{t_y}\right)^j \tag{A.16}$$

$$\Longrightarrow \left(T^+\right)^{jN_t} = P_+ h_1^j \left[\prod_{i=0}^{N_t-1} U_0(\vec{\mathbf{x}}, t_x + i)\right]^j (-1)^j \tag{A.17}$$

$$= P_+\, h_1^j\, W^j(\vec{\mathbf{x}}, t_x)(-1)^j \tag{A.18}$$

A couple of remarks here: In step two $(T^+)^j$ was extended with the exponent N_t. Then j and N_t were exchanged and after that we used the same argumentation for the operator U_0 like before. For the last step we used the definitions $h_1 \equiv z_+^{N_t}$ and $W(\vec{\mathbf{x}}, t_x) \equiv \prod_{i=0}^{N_t-1} U_0(\vec{\mathbf{x}}, t_x + i)$.

For the **second case** $t_x \neq t_y$ we have to fulfill the condition $t_y - t_x + jN_t > 0$, because now the time interval is not the same anymore and obviously discrete. So we again use Eq. (A.14) and extend the exponent now with the above mentioned condition. This leads to

$$\left(T^+\right)^{t_y - t_x + jN_t} = P_+ z^{t_y - t_x} h_1^j \begin{cases} W(\vec{\mathbf{x}}, t_x, t_y) W^j(\vec{\mathbf{x}}, t_y)\, (-1)^j & , \;\; t_x < t_y \\ W(\vec{\mathbf{x}}, t_x, t_y) W^{j-1}(\vec{\mathbf{x}}, t_y)\, (-1)^j & , \;\; t_x < t_y \end{cases} \tag{A.19}$$

with

$$W(\vec{\mathbf{x}},t_x,t_y)=\begin{cases}\prod_{i=0}^{t_y-t_x-1}U_0(\vec{\mathbf{x}},t_x+i)\;, & t_x<t_y\\ \prod_{i=0}^{N_t-t_x+t_y-1}U_0(\vec{\mathbf{x}},t_x+i)\;, & t_x\geq t_y\end{cases}\quad. \tag{A.20}$$

With the step function $\theta(0)=0$ all results can be summarized in one equation:

$$\sum_{j=1}^{\infty}\left(T^{+}\right)^{j}=\delta_{\vec{\mathbf{x}},\vec{\mathbf{y}}}\;P_{+}\Big[-\delta_{t_x,t_y}h_1W(\vec{\mathbf{x}},t_x)(\mathbb{1}+h_1W(\vec{\mathbf{x}},t_x))^{-1} \tag{A.21}$$

$$+z^{t_y-t_x}W(\vec{\mathbf{x}},t_x,t_y)(\mathbb{1}+h_1W(\vec{\mathbf{x}},t_x))^{-1}[\theta(t_y-t_x)-h_1\theta(t_x-t_y)]\Big] \tag{A.22}$$

It is noted that the same calculation also applies to T^{-}, with the difference that $z_{+}\rightarrow z_{-}$ and $W\rightarrow W^{\dagger}$. After discussing $T^{\pm}$ we finally can put all our results in the static operator, which was first calculated in Eq. (A.12).

$$Q^{-1}_{\text{stat}}(x,y)=\delta_{\vec{\mathbf{x}},\vec{\mathbf{y}}}\Bigg\{\delta_{t_x,t_y}\left[\mathbb{1}-P_{+}\frac{h_1W(\vec{\mathbf{x}},t_x)}{\mathbb{1}+h_1W(\vec{\mathbf{x}},t_x)}-P_{-}\frac{\overline{h}_1W^{\dagger}(\vec{\mathbf{x}},t_x)}{\mathbb{1}+W^{\dagger}(\vec{\mathbf{x}},t_x)}\right] \tag{A.23}$$

$$+\theta(t_y-t_x)\left[P_{+}\;z_{+}^{t_y-t_x}\frac{W(\vec{\mathbf{x}},t_x,t_y)}{\mathbb{1}+h_1W(\vec{\mathbf{x}},t_y)}-P_{-}z_{-}^{t_x-t_y}\overline{h}_1\frac{W^{\dagger}(\vec{\mathbf{x}},t_x,t_y)}{\mathbb{1}\overline{h}_1W^{\dagger}(\vec{\mathbf{x}},t_y)}\right] \tag{A.24}$$

$$+\theta(t_x-t_y)\left[-P_{+}\;z_{+}^{t_y-t_x}h_1\frac{W(\vec{\mathbf{x}},t_x,t_y)}{\mathbb{1}+h_1W(\vec{\mathbf{x}},t_y)}+P_{-}z_{-}^{t_x-t_y}\frac{W^{\dagger}(\vec{\mathbf{x}},t_x,t_y)}{\mathbb{1}\overline{h}_1W^{\dagger}(\vec{\mathbf{x}},t_y)}\right]\Bigg\} \tag{A.25}$$

For comparison with the literature, the static propagator is also written in the following way

$$Q^{-1}_{\text{stat}}=A^{+}_{x,y}+A^{-}_{x,y}+\gamma_0\big[B^{+}_{x,y}-B^{-}_{x,y}\big], \tag{A.26}$$

with

$$A^{+}_{x,y}=\frac{1}{2}\left[\mathbb{1}-\frac{h_1W}{\mathbb{1}+h_1W}\right]+\frac{1}{2}\delta_{\vec{\mathbf{x}},\vec{\mathbf{y}}}h_1^{\frac{t_y-t_x}{N_t}}\frac{W(t_x,t_y)}{\mathbb{1}+h_1W}[\theta(t_y-t_x)-h_1\theta(t_x-t_y)]$$

$$A^{-}_{x,y}=\frac{1}{2}\left[\mathbb{1}-\frac{\overline{h}_1W^{\dagger}}{\mathbb{1}+\overline{h}_1W^{\dagger}}\right]+\frac{1}{2}\delta_{\vec{\mathbf{x}},\vec{\mathbf{y}}}\overline{h}_1^{\frac{t_y-t_x}{N_t}}\frac{W^{\dagger}(t_x,t_y)}{\mathbb{1}+\overline{h}_1W^{\dagger}}\big[\theta(t_x-t_y)-\overline{h}_1\theta(t_y-t_x)\big]$$

and

$$B^{+}_{x,y}=-\frac{1}{2}\frac{h_1W}{\mathbb{1}+h_1W}+\frac{1}{2}\delta_{\vec{\mathbf{x}},\vec{\mathbf{y}}}h_1^{\frac{t_y-t_x}{N_t}}\frac{W(t_x,t_y)}{\mathbb{1}+h_1W}[\theta(t_y-t_x)-h_1\theta(t_x-t_y)] \tag{A.27}$$

$$B^{-}_{x,y}=-\frac{1}{2}\frac{\overline{h}_1W^{\dagger}}{\mathbb{1}+\overline{h}_1W^{\dagger}}+\frac{1}{2}\delta_{\vec{\mathbf{x}},\vec{\mathbf{y}}}\overline{h}_1^{\frac{t_y-t_x}{N_t}}\frac{W^{\dagger}(t_x,t_y)}{\mathbb{1}+\overline{h}_1W^{\dagger}}\big[\theta(t_y-t_x)-\overline{h}_1\theta(t_x-t_y)\big]. \tag{A.28}$$

Finally we can determine the static propagator as

$$\boxed{Q^{-1}_{\text{stat}}(x,y) \equiv A_{x,y} + \gamma_0 \, B_{x,y}} \tag{A.29}$$

with the definitions $A_{x,y} \equiv A^{+}_{x,y} + A^{-}_{x,y}$ and $B_{x,y} \equiv B^{+}_{x,y} - B^{-}_{x,y}$.

A.4 Expressing the terms $\operatorname{Tr}\frac{h_1 W}{\mathbb{1}+h_1 W}$ and $\operatorname{Tr}\frac{\overline{h}_1 W^\dagger}{\mathbb{1}+\overline{h}_1 W^\dagger}$ with Polyakov-Loops

We start with:

$$\begin{aligned}
\operatorname{Tr}\frac{h_1 W}{\mathbb{1}+h_1 W} &= \operatorname{Tr}\left[h_1 W(\mathbb{1}+h_1 W)^{-1}\right] \\
&= \operatorname{Tr}\left[h_1 W\left[\underbrace{\frac{1}{1+h_1 L+h_1^2 L^\star+h_1^3}}_{\equiv\frac{1}{Z}}\left(1+h_1 L-h_1 W+h_1^2 W^\dagger\right)\right]\right] \\
&= \frac{1}{Z}\left[h_1 \operatorname{Tr}(W)+h_1^2 L \operatorname{Tr}(W)-h_1^2 \operatorname{Tr}\left(W^2\right)+h_1^3 \operatorname{Tr}\left(W\,W^\dagger\right)\right] \\
&= \frac{1}{Z}\left[h_1 L+h_1^2 L^2-h_1^2 \operatorname{Tr}\left(W^2\right)+3h_1^3\right].
\end{aligned}$$

Here we used the identities $WW^\dagger = \mathbb{1}$ and $L = \operatorname{Tr} W$. Next we apply our formula for the term W^2, which is $W^2 = -\operatorname{Tr}\left(W^\dagger\right)\mathbb{1}+\operatorname{Tr}(W)W+W^\dagger$ [46]. After inserting this term into the equation and multiplying all terms out, we get the result

$$\operatorname{Tr}\frac{h_1 W}{\mathbb{1}+h_1 W} = \frac{h_1 L+2h_1^2 L^\star+3h_1^3}{1+h_1 L+h_1^2 L^\star+h_1^3}. \tag{A.30}$$

To get the other term from Eq. (3.32), we use exactly the same procedure again, changing only $L^\star = \operatorname{Tr} W^\dagger$ and $\left(W^\dagger\right)^2 = -\operatorname{Tr}\left(W^\dagger\right)\mathbb{1}+\operatorname{Tr}(W)W+W^\dagger$. It follows

$$\operatorname{Tr}\frac{\overline{h}_1 W^\dagger}{\mathbb{1}+\overline{h}_1 W^\dagger} = \frac{\overline{h}_1 L+2\overline{h}_1^2 L^\star+3\overline{h}_1^3}{1+\overline{h}_1 L^\star+\overline{h}_1^2 L+\overline{h}_1^3}. \tag{A.31}$$

A.5 Calculating $SU(3)$ integrals

To calculate the static or kinetic determinant, it was necessary to use certain integral techniques. Since we are dealing here with $SU(3)$ integrals, this section will deal with the calculation of these integrals. This calculation is based on Ref. [29]. If we want to calculate integrals in the partition function, we typically encounter integrals with the following generating functional

$$G(u,v) = \int \mathrm{d}P e^{u\,\mathrm{Tr}\,P} e^{u\,\mathrm{Tr}\,P^\dagger} \tag{A.32}$$

$$= \sum_{n,m=0}^{\infty} \frac{u^n}{n!}\frac{v^m}{m!}\,\mathcal{I}(n,m). \tag{A.33}$$

In the second step we used the series expansion of the exponential function, namely $\exp x \equiv \sum_{k=0}^{\infty} \frac{x^k}{k!}$. The expression $\mathcal{I}(n,m)$ stands for the moments of the one link integral for $G(u,v)$. Given from Ref. [47], we can use

$$G(u,v) = \sum_{p,q=0}^{\infty} \frac{2}{(p+q+1)!(p+q+2)!q!} \binom{3(p+q+1)}{p} (uv)^p (u^3+v^3)^q. \tag{A.34}$$

With the standard binomial theorem $(x+y)^n = \sum_{k=0}^{n} \binom{n}{k} x^{n-k}y^k$ or more precisely in the case $(u^3+v^3)^q$ above and after organizing the terms after $u^n v^m$ we obtain

$$G(u,v) = \sum_{p,q=0}^{\infty} \frac{2}{(p+q+1)!(p+q+2)!q!} \binom{3(p+q+1)}{p} \sum_{j=0}^{q} \binom{q}{j} u^{p+3j}\; v^{p+3q-3j} \tag{A.35}$$

$$= \sum_{n,m=0}^{\infty} \frac{u^n}{n!}\frac{v^m}{m!} \sum_{p,q=0}^{\infty}\sum_{j=0}^{q} \frac{2n!\; m!\; \delta_{n,p+3j}\; \delta_{m,p+3j-3j}}{(p+q+1)!(p+q+2)!q!} \binom{3(p+q+1)}{p}\binom{q}{j}. \tag{A.36}$$

Next we compare Eq. (A.36) with Eq. (A.33) and we find

$$\mathcal{I}(n,m) = \sum_{p,q=0}^{\infty}\sum_{j=0}^{q} \delta_{n,p+3j}\; \delta_{m,p+3q-3j} \frac{2n!m!}{(p+q+1)!(p+q+2)!q!} \binom{3(p+q+1)}{p}\binom{q}{j} \tag{A.37}$$

Kronecker deltas reduce the expression in Eq. (A.36) to a finite sum. The first Kronecker delta $\delta_{n,p+3j}$ implies the restriction for $p = n-3j$ and since $p \geq 0$ we find $n \geq 3j$. This relation implies an upper bound for the sum by $j \leq \lfloor \frac{n}{3} \rfloor$. So we can apply the first Kronecker delta and we get

$$\mathcal{I}(n,m) = \sum_{q=0}^{\infty}\sum_{j=0}^{\lfloor \frac{n}{3} \rfloor} \frac{\delta_{m,n+3q-6j}\; 2n!\; m!}{(n-3j+q+1)!(n-3j+q+2)!\; q!} \binom{3(n-3j+q+1)}{n-3j}\binom{q}{j}. \tag{A.38}$$

The remaining Kronecker delta in Eq. (A.38) written as $\delta_{n-m,6j-3q}$ which implies the following conditions for $\mathcal{I}(n,m)$:

$$\mathcal{I}(n,m) = \begin{cases} \neq 0 \ , & \text{if } (n-m) \mod 3 = 0 \\ = 0 \ , & \text{else} \end{cases}$$

This relation is also called the **triality constraint**. The Kronecker delta $\delta_{n-m,6j-3q}$ implies also for $q = 2j - \frac{n-m}{3}$, so the binomial factor is then $\binom{q}{j} = \binom{2j-\frac{n-m}{3}}{j}$. From the Kronecker delta we also obtain the resitriction for j, which is $j \geq \frac{n-m}{3}$ and since j must be non-negative, the lower bound must be $j \geq \max\left(0, \frac{n-m}{3}\right)$. Finally the last Kronecker delta can act on the sum now and we get the final result

$$\boxed{\mathcal{I}(n,m) = \sum_{j=\max\left(0,\frac{n-m}{3}\right)}^{\lfloor \frac{n}{3} \rfloor} \frac{T(n-m)\, 2n!\, m! \, \binom{3\left(n-j-\frac{n-m}{3}+1\right)}{n-3j} \binom{2j-\frac{n-m}{3}}{j}}{\left(n-j-\frac{n-m}{3}+1\right)!\left(n-j-\frac{n-m}{3}+2\right)!\left(2j-\frac{n-m}{3}\right)!}} \tag{A.39}$$

with the triality function

$$T(n) = \begin{cases} 1 \ , & \text{if } n \mod 3 = 0 \\ 0 \ , & \text{else} \end{cases}$$

The final result in Eq. (A.39) calculates the moments of $\mathcal{I}(n,m)$ as finite sums. In appendix of Ref. [47] are the lowest moments for $n, m \leq 10$ evaluated.

A.5.1 Some integrals over Polyakov-Loops

In this section, we list some integrals over Polyakov-Loop, which were important for the analysis.

$$\int \mathrm{d}L L^3 = 1$$
$$\int \mathrm{d}L L^6 = 5$$
$$\int \mathrm{d}L L^9 = 42$$
$$\int \mathrm{d}L \left(L^\dagger\right)^3 = 1$$
$$\int \mathrm{d}L \left(L^\dagger\right)^6 = 5$$
$$\int \mathrm{d}L \left(L^\dagger\right)^9 = 42$$
$$\int \mathrm{d}L L \left(L^\dagger\right) = 1$$
$$\int \mathrm{d}L L^2 \left(L^\dagger\right)^2 = 2$$
$$\int \mathrm{d}L L^3 \left(L^\dagger\right) = 6$$
$$\int \mathrm{d}L L^4 \left(L^\dagger\right)^4 = 23$$
$$\int \mathrm{d}L L^5 \left(L^\dagger\right)^5 = 103$$
$$\int \mathrm{d}L L \left(L^\dagger\right)^4 = 3$$
$$\int \mathrm{d}L L \left(L^\dagger\right)^7 = 21$$
$$\int \mathrm{d}L L^2 \left(L^\dagger\right)^5 = 11$$
$$\int \mathrm{d}L L^2 \left(L^\dagger\right)^8 = 98$$
$$\int \mathrm{d}L L^3 \left(L^\dagger\right)^6 = 47$$
$$\int \mathrm{d}L L^4 \left(L^\dagger\right)^1 = 3$$
$$\int \mathrm{d}L L^5 \left(L^\dagger\right)^2 = 11$$
$$\int \mathrm{d}L L^6 \left(L^\dagger\right)^3 = 47$$
$$\int \mathrm{d}L L^7 \left(L^\dagger\right)^1 = 21$$
$$\int \mathrm{d}L L^8 \left(L^\dagger\right)^2 = 98$$

Bibliography

[1] Wikipedia. Standard model. https://en.wikipedia.org/wiki/Standard_Model, 2020, Sep.

[2] Andre Roberge and Nathan Weiss. Gauge Theories With Imaginary Chemical Potential and the Phases of QCD. *Nucl. Phys. B*, 275:734–745, 1986.

[3] Jana N. Guenther. Overview of the QCD phase diagram: Recent progress from the lattice. *Eur. Phys. J. A*, 57(4):136, 2021.

[4] Edwin Laermann and Owe Philipsen. The Status of lattice QCD at finite temperature. *Ann. Rev. Nucl. Part. Sci.*, 53:163–198, 2003.

[5] Kenji Fukushima and Tetsuo Hatsuda. The phase diagram of dense QCD. *Rept. Prog. Phys.*, 74:014001, 2011.

[6] Szabolcs Borsanyi, Zoltan Fodor, Christian Hoelbling, Sandor D Katz, Stefan Krieg, Claudia Ratti, and Kalman K. Szabo. Is there still any T_c mystery in lattice QCD? Results with physical masses in the continuum limit III. *JHEP*, 09:073, 2010.

[7] Michael Cheng, Norman H. Christ, Min Li, Robert D. Mawhinney, Dwight Renfrew, Prasad Hegde, Frithjof Karsch, Meifeng Lin, and Pavlos Vranas. Finite temperature qcd using2+1flavors of domain wall fermions atnt=8. *Physical Review D*, 81(5), Mar 2010.

[8] Masataka Fukugita, Masanori Okawa, and Akira Ukawa. Finite Size Scaling Study of the Deconfining Phase Transition in Pure SU(3) Lattice Gauge Theory. *Nucl. Phys. B*, 337:181–232, 1990.

[9] D. T. Son and Misha A. Stephanov. QCD at finite isospin density. *Phys. Rev. Lett.*, 86:592–595, 2001.

[10] M. Asakawa and K. Yazaki. Chiral Restoration at Finite Density and Temperature. *Nucl. Phys. A*, 504:668–684, 1989.

[11] Philippe Chomaz. The nuclear liquid gas phase transition and phase coexistence. *AIP Conf. Proc.*, 610(1):167, 2002.

[12] David J. Gross and Frank Wilczek. Ultraviolet behavior of non-abelian gauge theories. *Phys. Rev. Lett.*, 30:1343–1346, Jun 1973.

[13] Philippe de Forcrand. Simulating QCD at finite density. *PoS*, LAT2009:010, 2009.

[14] Bastian B. Brandt, Gergely Endrodi, and Sebastian Schmalzbauer. QCD at finite isospin chemical potential. *EPJ Web Conf.*, 175:07020, 2018.

[15] Thomas D. Cohen. QCD functional integrals for systems with nonzero chemical potential. In *From Fields to Strings: Circumnavigating Theoretical Physics: A Conference in Tribute to Ian Kogan*, pages 101–120, 5 2004.

[16] A. B. Migdal. Pion fields in nuclear matter. *Rev. Mod. Phys.*, 50:107–172, Jan 1978.

[17] Sean Gavin, Andreas Gocksch, and Robert D. Pisarski. QCD and the chiral critical point. *Phys. Rev. D*, 49:R3079–R3082, 1994.

[18] Robert D. Pisarski and Frank Wilczek. Remarks on the chiral phase transition in chromodynamics. *Phys. Rev. D*, 29:338–341, Jan 1984.

[19] Benjamin Svetitsky and Laurence G. Yaffe. Critical Behavior at Finite Temperature Confinement Transitions. *Nucl. Phys. B*, 210:423–447, 1982.

[20] Robert D. Pisarski and Frank Wilczek. Remarks on the Chiral Phase Transition in Chromodynamics. *Phys. Rev. D*, 29:338–341, 1984.

[21] G. Boyd, J. Engels, F. Karsch, E. Laermann, C. Legeland, M. Lutgemeier, and B. Petersson. Thermodynamics of SU(3) lattice gauge theory. *Nucl. Phys. B*, 469:419–444, 1996.

[22] Francesca Cuteri, Christopher Czaban, Owe Philipsen, and Alessandro Sciarra. Updates on the Columbia plot and its extended/alternative versions. *EPJ Web Conf.*, 175:07032, 2018.

[23] Philippe de Forcrand and Owe Philipsen. The Chiral critical line of N(f) = 2+1 QCD at zero and non-zero baryon density. *JHEP*, 01:077, 2007.

[24] Andrea Pelissetto and Ettore Vicari. Relevance of the axial anomaly at the finite-temperature chiral transition in QCD. *Phys. Rev. D*, 88(10):105018, 2013.

[25] Y. Aoki, G. Endrodi, Z. Fodor, S. D. Katz, and K. K. Szabo. The Order of the quantum chromodynamics transition predicted by the standard model of particle physics. *Nature*, 443:675–678, 2006.

[26] Philippe de Forcrand and Owe Philipsen. The curvature of the critical surface (m(u,d),m(s))**crit(mu): A Progress report. *PoS*, LATTICE2008:208, 2008.

[27] Gert Aarts. Complex Langevin dynamics and other approaches at finite chemical potential. *PoS*, LATTICE2012:017, 2012.

[28] Christof Gattringer. New developments for dual methods in lattice field theory at non-zero density. *PoS*, LATTICE2013:002, 2014.

[29] Christof Gattringer. Flux representation of an effective Polyakov loop model for QCD thermodynamics. *Nucl. Phys. B*, 850:242–252, 2011.

[30] Silas R. Beane, Kostas Orginos, and Martin J. Savage. Hadronic Interactions from Lattice QCD. *Int. J. Mod. Phys. E*, 17:1157–1218, 2008.

[31] I. Montvay and G. Munster. *Quantum fields on a lattice*. Cambridge Monographs on Mathematical Physics. Cambridge University Press, 3 1997.

[32] Jean-Michel Drouffe and Jean-Bernard Zuber. Strong coupling and mean field methods in lattice gauge theories. *Physics Reports*, 102(1):1–119, 1983.

[33] Alexander S. Christensen, Joyce C. Myers, and Peter D. Pedersen. Large N lattice QCD and its extended strong-weak connection to the hypersphere. *JHEP*, 02:028, 2014.

[34] Jens Langelage, Stefano Lottini, and Owe Philipsen. Centre symmetric 3d effective actions for thermal SU(N) Yang-Mills from strong coupling series. *JHEP*, 02:057, 2011. [Erratum: JHEP 07, 014 (2011)].

[35] M. Neuman. *Effective Theory for Heavy Quark QCD at Finite Temperature and Density with Stochastic Quantization*. PhD thesis, Goethe University, 2015.

[36] M. Creutz. On invariant integration over SU(N). *AIP Journal of Mathematical Physics*, 19:2043, 1978.

[37] Owe Philipsen and Jonas Scheunert. QCD in the heavy dense regime for general N_c: on the existence of quarkyonic matter. *JHEP*, 11:022, 2019.

[38] Linda E. Reichl. *A Modern Course in Statistical Physics*. Wiley-VCH, Verlag Gmbh, 2016.

[39] Larry D. McLerran and Benjamin Svetitsky. Quark liberation at high temperature: A monte carlo study of su(2) gauge theory. *Phys. Rev. D*, 24:450–460, Jul 1981.

[40] John B. Kogut, Michael Snow, and Michael Stone. Mean Field and Monte Carlo Studies of SU(N) Chiral Models in Three-dimensions. *Nucl. Phys. B*, 200:211–231, 1982.

[41] F. Green and F. Karsch. Mean Field Analysis of SU(N) Deconfining Transitions in the Presence of Dynamical Quarks. *Nucl. Phys. B*, 238:297–306, 1984.

[42] V. M. Wiedemann. Mean Field Approach to Effective Polyakov Loop Theories. Master's thesis, Goethe University, 2019.

[43] Michael Fromm, Jens Langelage, Stefano Lottini, Mathias Neuman, and Owe Philipsen. Onset Transition to Cold Nuclear Matter from Lattice QCD with Heavy Quarks. *Phys. Rev. Lett.*, 110(12):122001, 2013.

[44] Jonas Glesaaen, Mathias Neuman, and Owe Philipsen. Heavy dense QCD from a 3d effective lattice theory. *PoS*, LATTICE2015:173, 2016.

[45] A. Schön. Effective heavy quark theory of strong coupling lattice QCD in 1+1 dimensions. Master's thesis, Goethe University, 2018.

[46] M. Salg. The deconfinement transition in an effective theory for heavy quark Lattice QCD to $\mathcal{O}(\kappa^4)$. Master's thesis, Goethe University, 2020.

[47] S. Uhlmann, R. Meinel, and A. Wipf. Ward identities for invariant group integrals. *J. Phys. A*, 40:4367–4390, 2007.

List of Figures

List of Tables

Declaration

I herewith declare that I have produced my master thesis on the topic of "*Mean field analysis of an effective Lattice theory for isospin and baryonic chemical potential*" independently and using only the tools indicated therein. In particular, all references borrowed from external sources are clearly acknowledged and identified.

I confirm that I have respected the principles of good scientific practice and have not made use of the services of any commercial agency in respect of my master.

Frankfurt am Main: _____ Signature: _____

Amine Chabane